NAVAL POSTGRADUATE SCHOOL
Monterey, California

THESIS

REMOTE NANOSATELLITE FORMATION DESIGNS WITH ORBIT PERTURBATION CORRECTIONS AND ATTITUDE CONTROL/PROPULSION SUBSYSTEM CORRELATION

by

Stephen D. Tomlin

June 21, 2000

Thesis Advisor: Brij N. Agrawal
Second Reader: Norm N. Sorenson

Approved for public release; distribution is unlimited.

REPORT DOCUMENTATION PAGE			Form Approved OMB No. 0704-0188
Public reporting burden for this collection of information is estimated to average 1 hour per response, including the time for reviewing instruction, searching existing data sources, gathering and maintaining the data needed, and completing and reviewing the collection of information. Send comments regarding this burden estimate or any other aspect of this collection of information, including suggestions for reducing this burden, to Washington headquarters Services, Directorate for Information Operations and Reports, 1215 Jefferson Davis Highway, Suite 1204, Arlington, VA 22202-4302, and to the Office of Management and Budget, Paperwork Reduction Project (0704-0188) Washington DC 20503.			
1. AGENCY USE ONLY *(Leave blank)*	**2. REPORT DATE** June 2001	**3. REPORT TYPE AND DATES COVERED** Master's Thesis	
4. TITLE AND SUBTITLE: REMOTE NANOSATELLITE FORMATION DESIGNS WITH ORBIT PERTURBATION CORRECTIONS AND ATTITUDE CONTROL / PROPULSION SUBSYSTEM CORRELATION			**5. FUNDING NUMBERS**
6. AUTHOR(S) Tomlin, Stephen D.			
7. PERFORMING ORGANIZATION NAME(S) AND ADDRESS(ES) Naval Postgraduate School Monterey, CA 93943-5000			**8. PERFORMING ORGANIZATION REPORT NUMBER**
9. SPONSORING / MONITORING AGENCY NAME(S) AND ADDRESS(ES) N/A			**10. SPONSORING / MONITORING AGENCY REPORT NUMBER**
11. SUPPLEMENTARY NOTES The views expressed in this thesis are those of the author and do not reflect the official policy or position of the Department of Defense or the U.S. Government.			
12a. DISTRIBUTION / AVAILABILITY STATEMENT Approved for public release; distribution is unlimited.			**12b. DISTRIBUTION CODE**

13. ABSTRACT ***(maximum 200 words)***

The innovative idea of distributing the functionality of current larger satellites among smaller, cooperative satellites has been sincerely considered for assorted space missions to accomplish goals that are not possible or very difficult to do with a single satellite. Additionally, the utilization of smaller satellites is maximized within formations and clusters to conduct missions such as interferometry and earth-sensing. This paper presents a methodology to describe, populate and analyze numerous formation designs employing the use of Hill's equations of motion to describe a formation's dynamics. These equations of motion are then programmed into a MATLAB code to produce Cartesian elements for input into a Satellite Tool Kit™ (STK) simulation that demonstrates numerous possible cluster formation designs. These simulations are then used to determine ΔV requirements for overcoming LEO-type perturbations that were modeled within STK's High Precision Orbit Propagator (HPOP).

Finally, components from two subsystems [Attitude Determination and Control (ADCS) and Propulsion], using the ΔV calculations from the simulation analysis and current advances in MicroElectroMechanical systems (MEMs) and nanosatellite technology, are presented based on a mass constraint of 10kg for the entire satellite.

14. SUBJECT TERMS Nanosatellite, Orbit Dynamics, Satellite Formation, Satellite Cluster, Satellite Propulsion, STK			**15. NUMBER OF PAGES** 136
			16. PRICE CODE
17. SECURITY CLASSIFICATION OF REPORT Unclassified	**18. SECURITY CLASSIFICATION OF THIS PAGE** Unclassified	**19. SECURITY CLASSIFICATION OF ABSTRACT** Unclassified	**20. LIMITATION OF ABSTRACT** UL

NSN 7540-01-280-5500

Standard Form 298 (Rev. 2-89)
Prescribed by ANSI Std. 239-18

THIS PAGE INTENTIONALLY LEFT BLANK

Approved for public release; distribution is unlimited.

REMOTE NANOSATELLITE FORMATION DESIGNS WITH ORBIT PERTURBATION CORRECTIONS AND ATTITUDE CONTROL/PROPULSION SUBSYSTEM CORRELATION

Stephen D. Tomlin
Lieutenant, United States Navy
B.S., Rensselaer Polytechnic Institute, 1994

Submitted in partial fulfillment of the
requirements for the degree of

MASTER OF SCIENCE IN ASTRONAUTICAL ENGINEERING

from the

NAVAL POSTGRADUATE SCHOOL
June 2001

Author: 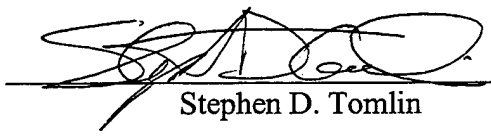
Stephen D. Tomlin

Approved by: 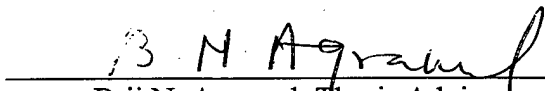
Brij N. Agrawal, Thesis Advisor

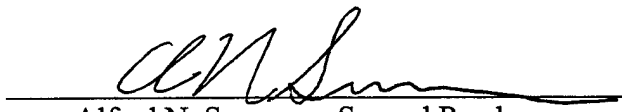
Alfred N. Sorenson, Second Reader

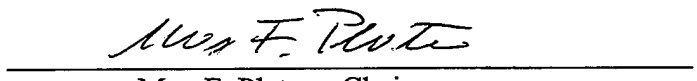
Max F. Platzer, Chairman
Department of Aeronautics and Astronautics

THIS PAGE INTENTIONALLY LEFT BLANK

ABSTRACT

The innovative idea of distributing the functionality of current larger satellites among smaller, cooperative satellites has been sincerely considered for assorted space missions to accomplish goals that are not possible or very difficult to do with a single satellite. Additionally, the utilization of smaller satellites is maximized within formations and clusters to conduct missions such as interferometry and earth-sensing. This paper presents a methodology to describe, populate and analyze numerous formation designs employing the use of Hill's equations of motion to describe a formation's dynamics. These equations of motion are then programmed into a MATLAB code to produce Cartesian elements for input into a Satellite Tool Kit™ (STK) simulation that demonstrates numerous possible cluster formation designs. These simulations are then used to determine ΔV requirements for overcoming LEO-type perturbations that were modeled within STK's High Precision Orbit Propagator (HPOP).

Finally, components from two subsystems [Attitude Determination and Control (ADCS) and Propulsion], using the ΔV calculations from the simulation analysis and current advances in MicroElectroMechanical systems (MEMs) and nanosatellite technology, are presented based on a mass constraint of 10kg for the entire satellite.

THIS PAGE INTENTIONALLY LEFT BLANK

TABLE OF CONTENTS

THIS PAGE INTENTIONALLY LEFT BLANK

LIST OF FIGURES

THIS PAGE INTENTIONALLY LEFT BLANK

LIST OF TABLES

THIS PAGE INTENTIONALLY LEFT BLANK

LIST OF SYMBOLS

a	semimajor axis
C_d	drag coefficient
C_{eff}	effective exhaust velocity
δ	angle that defines shape and orientation of suborbit plane
e	eccentricity
E	eccentric anomaly
ϕ	rotary angle
h	angular momentum
η	dimensionless pattern generator scale factor
i	inclination
I_{bit}	minimum impulse bit
I_{sp}	specific impulse
κ	elevation angle
λ	lateral angle
M	mean anomaly
μ	gravitational parameter ($398{,}600.441\ 5\ km^3/(solar\ sec)^2$)
ν	true anomaly
θ	phase angle of satellite (*measured clockwise from the cross-track(z) direction*)
q	orbit decay rate
r	radius of the formation

$\boldsymbol{r}$	position of remote from Earth (vector)
ρ	scale factor for formation creation
$\boldsymbol{R_e}$	radius of Earth
$\boldsymbol{R_p}$	radius of planet
$\boldsymbol{R}$	position of mothersat from Earth (vector)
t	time
T	thrust
u	angle from line of nodes to radial vector ($w + v$)
$\mathbf{v}$	velocity vector
w	argument of perigee
ω	mean motion
ω_e	rotation rate of the Earth (*0.000 072 921 158 553 0 rad/solar sec*)
Ω	right ascension of the ascending node
x	radial difference
y	along-track difference
z	cross-track difference
ΔV	velocity increment / 'delta-V'

ACKNOWLEDGMENTS

Of all the help, support and inspiration I received writing this paper, I wanted to first thank my wife Kimberly who has affectionately encouraged, assisted and loved me enough to enable my completion of this project. Without your help I would be stuck in more ways than one, thank you for the smiles, the laughter and the unwavering love.

To my three boys, Joshua, Daniel and Adam, I am truly blessed to be your father and I thank you guys for waiting patiently at the chess table, train table, and changing table respectively!

Also I wanted to express my sincere thanks to all my family members and friends who helped through words of prayer and encouragement to show me that anything is possible, and that a true faith and a loving family is all that is important. Thank you especially to Professor Brij Agrawal, Dr. Norm Sorenson, Dave Cook, and all the OCFers.

I also wanted to express my sincere thanks to Jon Strizzi, who took the time to read and critique this paper. Thank you for the time spent in reading, proofing and evaluating it with me afterwards. It was certainly the best review I got, thanks! And also to Jeff King who helped with his far superior knowledge of MATLAB. Thank you for the time spent and hopefully your part of the puzzle in this field will fit nicely!

Finally and most important, I thank my heavenly Father who has made possible, through His blessing and grace, my wonderful family, my blessed life and the ability to receive words of knowledge, wisdom and love. Without Him I would be building in vain.

THIS PAGE INTENTIONALLY LEFT BLANK

I. INTRODUCTION

> Nanotechnology provides the capability to manipulate matter at the atomic level. In the future, we will measure the way we design and build our systems by the atom, not by the pound. Today, we are developing material systems, at the molecular level, that are 100 times stronger than steel at 1/6 the weight. We will also develop sensors and detectors capable of responding to a single photon of light or the stimulus from a single electron. Using nanotechnology, we will build systems on a scale 1000 times smaller than today -- at true molecular level. They will be based on concepts emerging from biology, quantum mechanics and chemistry, all of which have no current parallel. [Ref 1]

A. NANOTECHNOLOGY PHENOMENON

Commercially and militarily, space systems based on MicroElectroMechanical systems (MEMS), nanoscale design and materials, low power quantum electronics, and high bandwidth photonics are of special interest, as are the demonstrations of space subsystems based on these technologies. Significant reductions in individual spacecraft mass and cost, large gains in capabilities and robustness, and novel architectures involving large constellations and closely coupled spacecraft are expected with the introduction of these technologies. Novel spacecraft architecture concepts for Earth orbiting missions including communication, navigation, remote earth-sensing, and monitoring of the local space environment that can be created with the introduction of micro/nano-technologies will be outlined briefly below.

B. DEFINING THE STARTING LINE

First of all, it is worth defining what we mean by a small satellite. The spirit of the current small satellite world is encompassed by the slogan 'Faster, Better, Smaller, Cheaper'. Small satellite projects are characterized by rapid development when compared with the conventional space industry, often ranging from six to thirty-six months. Leading-edge technology is routinely included in order to provide innovative

solutions, permitting lighter satellite systems to be designed inside smaller volumes. Frequently, traditional procedures, with roots in the military and manned space programs, can no longer be justified, and low cost solutions are favored to match the reducing space budgets. So in many ways it is the philosophy, and not the size or mass of the satellite that matters.

Many terms are used to describe this rediscovered class of satellites, including SmallSat, Cheapsat, MicroSat, MiniSat, NanoSat and even PicoSat. The US Defense Advanced Research Projects Agency (DARPA) refers to these as LightSats, the U.S. Naval Space Command as SPINSat's (Single Purpose Inexpensive Satellite Systems), and the U.S. Air Force as TACSat's (Tactical Satellites). Nevertheless, in recent years a general method of classifying satellites in terms of deployed mass has been generally adopted (see Table 1.1).

The boundaries of these classes are an indication of where launcher or cost tradeoffs are typically made, which is also why the mass is defined including fuel (i.e. 'wet mass'). Although the satellites in the 500-1000kg are typically designated as a 'small satellite', this causes confusion and until a better term appears it will be defined here as a medium sized satellite.

Group name	Wet Mass	
Large satellite	>1000kg	
Medium-sized satellite	500-1000kg	
Mini satellite	**100-500kg**	**Small Satellites**
Micro satellite	**10-100kg**	
Nano satellite	**1-10kg**	
Pico satellite	**0.1-1kg**	
Femto satellite	**<100g**	

Table 1.1 Satellite Classifications

The mass distribution for small satellites plotted in Fig. 1.1 illustrates that there ıre no clear mass boundaries, although there is a general lack of spacecraft in the 100-:00kg class. The positive sloping line in the figure depicts a gradual increase in the mass ›f launched satellites. Although this trend will continue as heavier satellites are launched vithin the next few years, the number of smaller satellites launched should start to emove this trend.

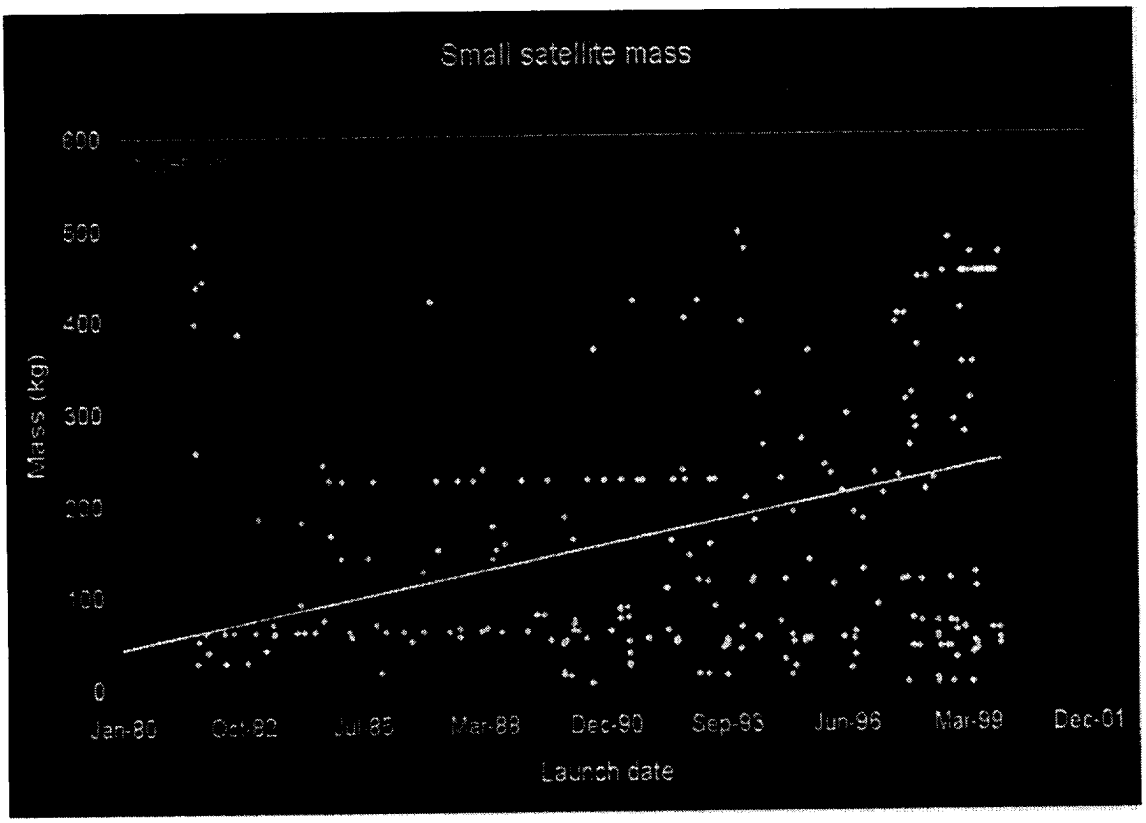

Figure 1.1 Small Satellite Launch Mass

C. CURRENT AND FUTURE EMPHASIS

Few modern Nano and Pico-Satellites weighing less than 10kg have been aunched, although there is considerable interest in this area as advanced microsat echnology is applied to miniaturize satellite systems even further. Some launched nicrosats almost fall into this category with weights of 11-14kg, most notably the

AMSAT microsat-series [Ref 2]. These satellites are cubical in shape and measure less than 150mm on each side.

Nanosatellites are attractive to many educational institutions to get involved in space, as commonly available technology now makes this type of satellite feasible and most importantly affordable. Although operational picosatellites weighing less than 1kg are still some time off, Aerospace Corporation just recently launched a set of picosatellites (see Chapter 2A: JAWSAT below). Increasingly, micro and nanotechnology makes it possible to fabricate entire satellite sub-systems, and possibly entire satellites on a chip. Considerable effort is being spent on these Femtosatellites weighing less than 0.1kg, with applications in remote inspection, distributed measurement and disposable sensors.

For Nanosatellites, autonomous operation using a single on-board computer is feasible, making use of technology developed for laptop and palmtop computers. To minimize mass, active attitude and orbit control are often ignored, and omni-directional antennas are employed. The main limits are set by the downlink and power generation systems. The downlink data rate is limited by the orbit average power generation, and has to be operated at low data rates, or in burst mode.

The key to the successful development of nanosatellites and constellations is advanced technology. Each of the many enabling technologies toward nanotechnology represents a breakthrough in performance, capability, or application in a unique way. This technological challenge is formidable, since currently, the smallest "full-service" microspacecraft weighs 100 kg (220 lb) or more - size must be reduced by almost a factor of five. This will require revolutionary advances in microelectronics and spacecraft component technologies.

In addition, at present day, almost all space missions are flown as single spacecraft. This is because controlling spacecraft in flight is a very complex process. The problem of flying several spacecraft as one system is further compounded by the complex communication path from a constellation of spacecraft in flight high above Earth with communication stations on the ground. In order to work properly, the spacecraft will have to behave "intelligently" -- autonomously staying in constant contact with each other,

sharing information, and re-configuring onboard instruments and systems to behave as a single unit.

D. SIZE OBSTACLES

A fundamental problem in spaceflight is spacecraft size. It is very expensive to place satellites into space. For example, using expendable cost with eight launches a year for the Space Shuttle, it costs about $13,200 per kilogram ($6,000 per pound) to deploy a payload into low-Earth orbit. As a result, engineers try to design spacecraft to be as small as possible. It has been estimated that satellites using nanotechnology could measure 15 inches wide by 2 inches thick and weigh about 2 pounds. These satellites would then require smaller and therefore less expensive launchers. [Ref. 3]

Most Earth-observing spacecraft with science payloads weigh in excess of 1,000 kg (2,200 lbs). Microsatellites are much smaller, typically in the 100 kg (220 lb) or larger range. Nanosatellite are even smaller -- in the sub-20 kg (44 lbs) range. Small spacecraft are nothing new. In fact, the first satellite launched into space, Sputnik, weighed only about 90 kg (180 lbs). However, small spacecraft even today are very limited in their capabilities. Typically they lack any propulsion, possess only limited ability for attitude control, and carry one single-function payload.

What is needed is a new era of "smart", miniature spacecraft that will be "full service", meaning they will carry a wide range of spacecraft services including guidance, navigation and control, attitude control, propulsion, high bandwidth and complex communication functions.

Nanosatellites not only reduce launch costs, but they also reduce the risks associated with flying missions. Currently, several instruments and payloads are flown on a single, large spacecraft. A single instrument or system failure may severely degrade or disable the entire mission. Constellations of numerous spacecraft, each carrying complementary instruments reduce the risk of an entire mission failing if one system or instrument fails.

E. CONCEPTS OF THE AEROSPACE CORPORATION

Most of the radical new concepts for building and using spacecraft represented by the nanosatellite concept were developed at The Aerospace Corporation and formally introduced in a paper, "The Concept of 'Nanosatellite' for Revolutionary Low Cost Space Systems," presented at the 44th International Astronautical Federation Congress in Graz, Austria, in 1993.

Authors included Robinson, Siegfried Janson, Ph.D., -- who coined the term nanosatellite and originated the concept [Ref 3] -- and Henry Helvajian, Ph.D., a senior scientist in the microtechnology center and editor of the just-published book, "Microengineering Aerospace Systems."

A series of reports written by Helvajian, Janson, and Robinson and issued after the 1993 conference presented the details on how to design, build, power and maneuver nanosatellites. These nanosatellite technologies are now being explored by a number of national and international research organizations in addition to The Aerospace Corporation

The First International Conference on Integrated Micro/Nanotechnology for Space Applications was hosted jointly by the Aerospace Corporation and Johnson Space Center in Houston, from October 30th through November 3rd 1995. The purpose of the conference was to bring together scientists and engineers from the fields of microtechnology, nanoelectronics and space technology to explore the possibilities for applying newly emerging capabilities in microtechnology to space operations. The evolution of microelectronic technology coupled with the growth of MEMS in the past 4-5 years has had a significant impact in the commercial terrestrial sector. This influence can be evidenced particularly in sensor, optical switching and mass data storage applications that have been inserted into major industries such as transportation, medicine, telecommunications and computers. The focus of this conference was to anticipate and extend the incorporation of nanoelectronics and MEMS into Application Specific Integrated Microinstruments (ASIMs) in order to revolutionize the development of space systems.

F. THE SCOPE

This paper sets out to introduce, explore and design nanosatellite formation designs with their required orbital dynamics. Chapter two will introduce past and current systems that are based on novel nanosatellite concepts. Numerous systems will be covered in areas ranging from experimental military designs to innovative student-driven ideas and future-looking commercial enterprises, all expecting to capture the quickly developing realm of 'smaller, faster, cheaper' with regards to nanosatellite technology.

This paper presents a methodology to describe, populate and analyze numerous formation designs employing the use of Hill's equations of motion to describe a formation's dynamics. These equations of motion are then programmed into a MATLAB code to produce Cartesian elements for input into a Satellite Tool Kit™ (STK) simulation that demonstrates numerous possible cluster formation designs. After utilizing MATLAB and STK to create formation simulations modeled within STK's High Precision Orbit Propagator (HPOP), low-earth orbit (LEO) perturbations will be analyzed to understand the required delta-V (ΔV) to maintain the formation within given dimensional criteria.

Finally, components from two subsystems [Attitude Determination and Control (ADCS) and Propulsion], using the ΔV calculations from the simulation analysis and current advances in MicroElectroMechanical systems (MEMs) and nanosatellite technology, are presented based on a mass constraint of 10kg for the entire satellite.

THIS PAGE INTENTIONALLY LEFT BLANK

II. LITERATURE REVIEW: PAST AND CURRENT SYSTEMS

A. PAST SYSTEMS

1. 1958

The first U.S. earth satellite, Explorer I, was almost the first nanosatellite by today's standards. Launched by a modified Army Ballistic Missile Agency Jupiter-C on February 01, 1958 it, containing the upper stage, measured 2.03m long and 150mm in diameter, and with a mass of 13.6kg and an orbit of 347x1,859 km at 33.2 deg inclination. Explorer I, developed by the Jet Propulsion Laboratory, carried the U.S.-IGY (International Geophysical Year) experiment of James A. Van Allen and resulted in the discovery of the radiation belt around the earth [Ref. 4]. Although most US satellites to follow would weigh more and become bigger in size, there was one that could be considered the 'forefather' of today's nanosatellites: Vanguard-1.

Although the first official 'nanosatellite' would not appear for another thirty years, the first satellite launched in the 1-10kg mass range is ironically the oldest satellite still orbiting Earth. Originally, a simple nose cone was to be carried on Vanguard-1, but in July of 1957 it was decided that a small 1.47-kg (3.25 pound) test satellite would be used instead to exercise the tracking stations (see Fig. 2.1).

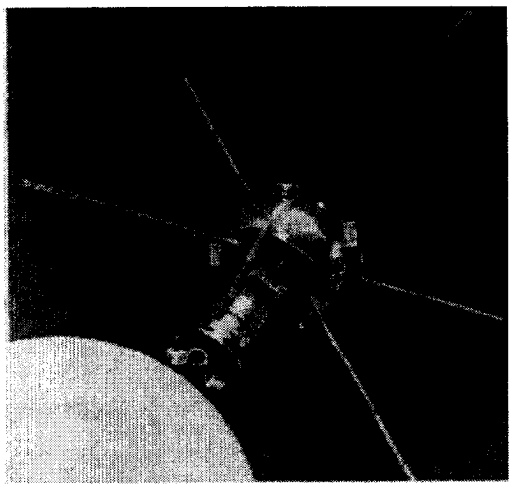

Figure 2.1 Vanguard-1

Launched March 17, 1958 into an elliptical (656x3866 km), 34.25 deg inclination orbit, this test satellite would consist of a simple 16 centimeter (6.4 inch) polished aluminum alloy sphere equipped with two transmitters operating at frequencies around 108 MHz. Although the Vanguard 1 satellite must be looked at as a test satellite its technical and scientific results is impressive. Technically its purpose was to test and evaluate solar cells, satellite terminal design and on board instrumentation. All these test objectives were met. The solar cells worked so well that its transmitters were active for six years, (interfering the 108 MHz frequency) well beyond the expected lifetime. The scientific results were also a success. As Soviet authorities and even some in the West scoffed at the diminutive size of Vanguard 1 and its lack of sophisticated instrumentation, it proved to be a very useful tool. Analysis of the motion of Vanguard 1 established the fact that the earth is not spherical but has a bulge, disclosing an unsuspected stress deep within the earth. These measurements indicated that there was large-scale convection taking place inside the Earth, which supported the emerging theories of continental drift and sea floor spreading. Analysis of the drag exerted by the atmosphere on Vanguard 1 proved the atmosphere to be far more extensive and variable than previously believed. Perturbations in Vanguard 1's orbit also led to a more refined estimate of the Earths oblateness. [Ref. 5]

2. 1990-1995

On September 03, 1990 China launched two atmospheric balloons (1990-081B/C), weighing 4kg each to measure the magnetosphere. QQW1 was launched into a 775x804 km orbit at 99 degrees and decayed on March 1, 1991. QQW2 was launched into an 833x886 km orbit at 99 degrees and decayed on July 24, 1991.

Also on two occasions in mid-1990 (February 03, 1994, February 04, 1995), a series of spherical objects were released from the shuttle, typically in pairs. These Orbital DEbris RAdar Calibration Spheres (ODERACS) were a few centimeters in diameter, and were intended to provide calibration for radar echoes. Appendix 2.1 provides the data on these objects.

3. 1995-2000

A commemorative functioning replica of the original Sputnik was deployed from the MIR space station (SPUTNIK-40 – *aka Sputnik-II, PS-2, RS-17, Sputnik Jr.*, 1997-058C, 24958) during an extravehicular activity (EVA) by Russian cosmonauts Anatoly Solovyov and Pavel Vinogradov on November 03, 1997. It was therefore in a 383x391 km orbit inclined at 51.6 degrees. It originally arrived via a Progress automated cargo rocket on October 9th. The satellite was 1/3 scale and weighed only 3kg and was built by French students from the l'Aeroclub of France (radio transmitter), staff from the Russian Aeronautical Federation (structure), and funded by various sponsors in the space industry. It stopped transmitting on the December 29, and decayed on the May 21, 1998.

The first satellites launched from a submarine were TUBSAT-N (1998-042A) and TUBSAT-N1 (1998-042B). The 8kg TUBSAT-N and the 3kg TUBSAT-N1 (see Fig. 2.2) were two nanosatellites launched on July 07, 1998 as a satellite cluster from a Russian nuclear powered submarine with a Shtil-1 converted missile in the Barents Sea, and was reported to have cost on the order of $100k (US$1998). The satellites were separated in orbit via telecommand and were placed into a 400x776 km orbit inclined at 78.9 degrees.

Figure 2.2 TUBSAT-N (bottom box) / -N1 (top plate)

The spacecrafts were flat-box shaped with a solar panel on the largest face, and each contained three different experimental payloads provided by the Technical University of Berlin (TUB): reaction wheel performance, star sensor performance, and

store and forward communication. The latter payload consisted of four independent communication transceivers for store and forward communication with a baud rate of 1200 and 2400 baud. Two transceivers worked in the 2m-frequency band, the other two in the 70-cm frequency band with FFSK (Fast Frequency Shift Keying) modulation. An additional downlink transmitter with 9600 Baud GMSK (Gaussian Minimum Shift Keying) modulation was available. The attitude control of TUBSAT-N consisted of two magnetic coils, a magnetometer, a reaction wheel and a star sensor. All attitude control devices were also developments of the Technical University of Berlin. Electrical power was provided by 9 NiCd-battery cells of 5 Ah (SANYO). The battery cells were connected serially and provided an unregulated bus voltage from 9 to 13 V. The current utilization of the nanosatellites is being used for tracking medium-sized and large mammals, stolen cars and to collect data from autonomous buoys for earth environmental observation. These buoys are located in the northern Atlantic Ocean near the Canary Islands.

A second sputnik, Sputnik-41 (*aka RS-18*, 1998-062C), was launched from the MIR spacestation into a 313x318 inclined orbit at 51.7 degrees on the November 10, 1998. A Progress-M40 cargo rocket delivered it to MIR on the October 25, 1998. It was financed by the Aeroclub de France, and built by French and Russian students. Sputnik-41's 200mW transmitter broadcasted pre-recorded voice greetings in French, English, and Russian. The spacecraft measured 230mm in diameter, and weighed 4kg. It decayed from orbit on the 11th January 1999.

The third "junior" sputnik, RS-19 (*aka Sputnik-Jr. 3rd*, 1999-015C), was launched from the MIR spacestation by Jean-Pierre Haignere during a spacewalk on the 16th April 1999. A Progress-M41 cargo rocket delivered it to MIR on the 2nd April 1999. Like earlier spacecraft in this series, it was supposed to transmit simple messages, however the spacecraft was launched "switched off", as advertising messages by a commercial company (Swatch) were carried in breach of International Telecommunication Union (ITU) regulations regarding amateur bands [Ref 6].

4. 2000 – Present

a. JAWSAT

On January 26, 2000 an OSPSLV (Orbital Suborbital Program Space Launch Vehicle) carried several microsatellites within a payload adapter called JAWSAT, developed jointly by the U.S. Air Force and Weber State University in Utah. Those satellites included FalconSat, an experimental satellite built by the U.S. Air Force Academy, ASUSat 1, built by students at Arizona State University; the Optical Calibration Sphere Experiment, an inflatable 3.5-meter (11.5-foot) balloon built by L'Garde for the Air Force Research Laboratory that served as a target for low-powered ground-based lasers; and Opal, a Stanford University satellite that, in turn, deployed six smaller "picosatellites" built by Santa Clara University, the Aerospace Corporation, and ham radio operators.

In addition to those satellites, JAWSAT included two other payloads that remained attached to it after launch. The Plasma Experiment Satellite Test (PEST), provided by NASA's Marshall Space Flight Center, studied plasma found at orbital altitudes, while Weber State's Attitude Control Platform tested a low-cost three-axis stabilization system. The launched satellites are covered below in more detail.

A tethered set of Picosatellites, DARPA Picosat (OPAL-#1&2), built by the Aerospace Corp. at Rockwell and funded by DARPA and UCLA weighing just 0.5kg and measuring 100x750x250mm each (see Fig. 2.3), launched from the OPAL microsatellite. They were deployed on February 6th, and communications were established 24 hours later. Gold strands in the tether were instrumental in radar tracking the pair. The spacecraft performed basic tests on MEMS RF switches. The spacecraft primary batteries (lithium thionyl chloride) ran out by February 10th.

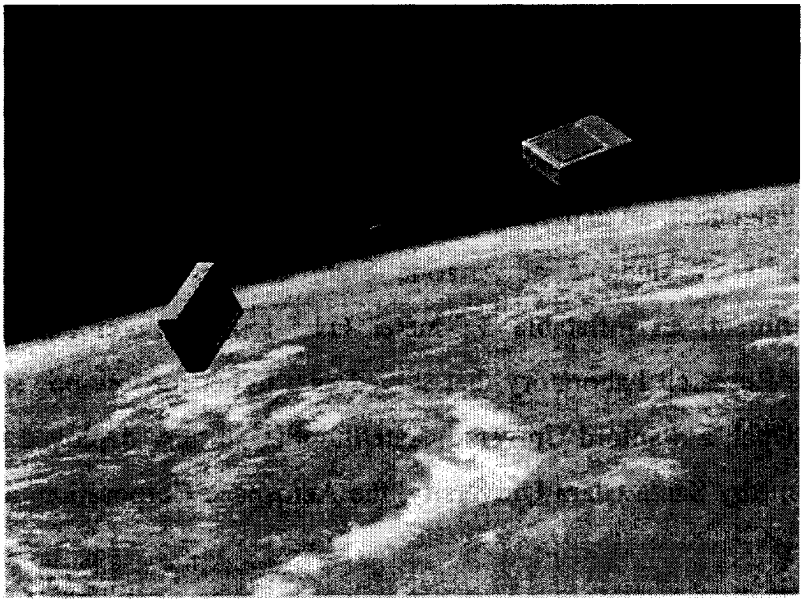

Figure 2.3 Aerospace tethered picosatellites (artist interpretation)

A picosatellite named after the Greek Goddess of the moon, the ARTEMIS Picosat (OPAL-#3&4, Thelma and Louise), weighed just 0.5kg and was built in a 5400 hour effort over a period of 10 months by an exclusively female team of 7 Santa Clara University students. The spacecraft employed a 68HC11 microcontroller, AA battery cells and GaAs solar cells. It was designed for one week of operations and was not attitude stabilized. It carried a Very Low Frequency (VLF) receiver. The spacecraft were deployed on February 11th, and were reported not to be operational. [Ref. 7]

MASAT, the Miniature Amateur Satellite, and STENSAT, NASA's amateur radio picosatellite built by Goddard Space Flight Center (GSFC), deployed on February 12th from the OPAL microsatellite. MASAT (OPAL-#5, JAK) was a picosatellite weighting just 0.5kg, and STENSAT (OPAL-#6) weighed in at just 0.25kg. Both spacecraft were reported not to be operational.

ASUSAT-1 was a 5kg nano-satellite designed and built at Arizona State University. It carried GPS, a camera, and a radio amateur FM repeater that only operated when requested on the uplink. The batteries failed to charge and therefore the satellite operated for approximately 15 hours during which telemetry was received, and is no longer operational.

b. SNAP-1

SNAP-1 (2000-033C, 26385) is a 6.5kg nanosatellite developed by Surrey Satellite Technology Limited (SSTL) and the Surrey Space Centre (SSC) in the UK (see Fig. 2.4). The spacecraft was launched as a piggyback ride on June 28, 2000 on a COSMOS-3M launcher from Plesetsk, together with the Tsinghua-1 microsatellite (China) and the Nadezhda-06 (Russia) primary payload. It was placed into a 684x707 km orbit inclined at 98.13 degrees. It carries a remote inspection payload, and an intersatellite link to communicate with Tshinghua-1. It carries a Butane propulsion system with a 3m/s capability. Further information will be presented on this satellite in Chapter 4 with regards to nanosatellite subsystem design. The spacecraft is still reported to be operational.

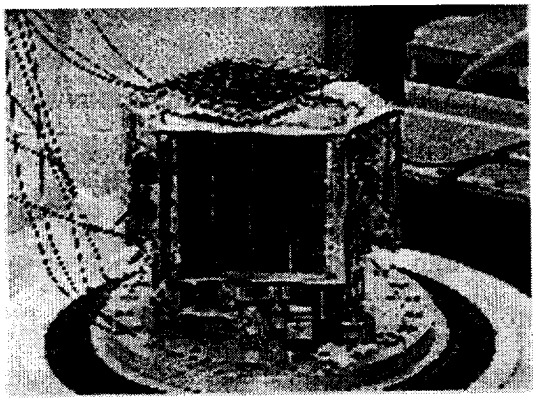

Figure 2.4 SNAP-1 from SSTL (UK)

c. Munin

Munin (2000-0, 26621A) is a Swedish 6kg satellite (7.5kg including separation system) to measure the electron and ion distribution in the aurora ovals and was launched into a 698x1800 km orbit. The satellite carries a spectrometer (DINA, Detector of Ions and Neutral Atoms), is cubic in shape and measures 200x200x250mm. The Swedish Institute of Space Physics (IRF) and the Dept. of Space Physics of Umeå University (RYP) designed the satellite. Munin was launched from VAFB, together with

EO-1 (Earth Observing-1), and SAC-C ('Satelite de Aplicaciones Cientificas'-C). The last contact with Munin was February 12, 2001.

B. STUDENT SATELLITE PROJECTS

In recent years, an increased effort to design, build, and operate small satellites has taken place in universities and laboratories all over the world. These microsatellites and nanosatellites provide numerous flight opportunities for science experiments at a fraction of the cost of larger traditional missions. In addition, there has been an increasing trend towards international cooperation on space projects. Tomorrow's engineers will find themselves working in an international environment for space progress to continue. Appendix 2.2 lists the most current educational establishments known to be involved in small spacecraft projects.

1. SSETI - Student Space Exploration & Technology Initiative

The European Space Agency (ESA) has started this ambitious educational project to involve students into the building of satellites: "...The main objective of this initiative is to create a network of students, educational institutions and organizations (on the Internet) to facilitate the distributed design, construction and launch of (micro)-satellites and potentially more complex projects such as a moon-lander [Ref. 8]." The first distribution round of the sub-systems resulted in the following distribution:

- AOCS: *Instituto Superior Técnico, Portugal*
- Communication: *UNICAL, Cosenza, Italy*
- Ground stations: *Instituto Superior Técnico, Portugal*
- Instruments: *University of Florence, Italy*
- Lander, Avionics: *Escola Politecnica Superior at Universitat de Girona, Spain*
- Mechanism: *EPFL(Lausanne), Switzerland*
- Mission Analysis: *University of Zaragoza, Spain*
- On-Board Data Handling (OBDH):

University of Newcastle, UK

- Power: *Euroavia-Napoli, Italy*
- Programmatic: *University of Stuttgart, Germany*
- Propulsion: *University of Stuttgart, Germany*
- SSETI Infrastructure: *Escola Politecnica Superior at Universitat de Girona, Spain*
- Simulation: *TU Vienna, Austria*
- Structures/Configuration:
  University of the Basque Country, Spain
- Structures/Structural calculations:
  Kingston University, UK
- Thermal: *Manchester University, UK*

2. University nanosatellite program

The Air Force Office of Scientific Research (AFOSR), NASA, and the Defense Advanced Research Projects Agency (DARPA) are jointly funding 10 universities with grants of $50k/year over two years to design and assemble 10 nanosatellites (~10kg). The universities will conduct creative low-cost space experiments to explore the military usefulness of nanosatellites in such areas as formation flying, miniature bus technologies, enhanced communications, miniaturized sensors, attitude control, distributed satellite capabilities and maneuvering. The satellites are planned to launch mid-2002. The 10 university nanosatellites provide a broad range of technology demonstrations in the areas of miniature spacecraft subsystem components and formation flying. There are also numerous science measurements and experiments in such areas as GPS scintillation, solar wind, magnetic fields, and upper atmosphere ion density.

The Air Force Research Laboratory (AFRL) is developing a deployment structure, securing a launch, and providing such advanced microsatellite hardware as high efficiency solar cells and micropropulsion units. NASA Goddard has also teamed with the universities to provide approximately $1.2M funding to demonstrate such formation flying technologies as advanced crosslink communication and navigation hardware and

flight control algorithms. Numerous industry partners are also supporting the universities with hardware and design and testing services.

This program has the potential to provide significant payoff for very modest funding by DoD and NASA given the broad university resources being applied and support by industry partners. If these flight demonstrations are successful, it is very likely government sponsorship can be secured for follow-on launches of nanosatellites built by universities and other agencies.

a. Three Corner SAT

This project is a joint effort between Arizona State University (ASU), University of Colorado at Boulder (CU), and New Mexico State University (NMSU). Aptly named Three Corner Sat (3^ Sat), the proposed constellation of three identical nanosatellites will demonstrate stereo imaging, formation flying/cellular-phone communications, and innovative command and data handling. In addition, each University in the 3^ Sat constellation has the opportunity to fly an individual unique payload should it desire. [Ref. 9]

b. ION-F

Utah State University, University of Washington, and Virginia Polytechnic Institute are designing and developing a system of three 10-kg spacecraft to investigate satellite coordination and management technologies and distributed ionospheric measurements. The three will coordinate on satellite design, formation flying and management mission development, and science instruments and mission. Advanced hardware for distributed space system to be demonstrated includes micro-pulsed plasma thrusters (μPPT), gimbaling magnetic attitude control, and an advanced tether system. In addition, an Internet based operations center will be designed to enable each university to control its satellite from its own remote location. ION-F will focus on mission objectives that would benefit TechSat 21 and future Air Force and NASA missions. In addition,

industrial (SDL, Primex, Honeywell) support has been identified, including funding for students, hardware, and satellite design support. [Ref. 10]

c. Emerald

Spacecraft formation flying is an evolving technology with vast scientific, military, and commercial potential that ranges from enhanced mission performance to radical reductions in operations cost. As part of the TechSat 21 University Nanosatellite Program, Stanford University and Santa Clara University are jointly developing EMERALD, a low cost, two-satellite mission for validating formation-flying technologies.

Stanford's SSDL (Space Systems Development Lab) and Santa Clara University's SCREEM (Santa Clara Remote Extreme Environment Mechanisms Laboratory) will work as a unified team to develop, construct, test and eventually operate the EMERALD spacecraft. The formation flying experiments will be coordinated through Stanford's ARL (Aerospace Robotics Lab)

The EMERALD Mission is divided into three distinct stages that progress from a simple single satellite to two free flying satellites in a coarse formation. Using a building block experimental strategy, the research payloads first will be characterized in isolation. Then, they will be coordinated and combined to permit simple demonstrations of fundamental formation flying control functions such as relative position determination and position control. At release, the two spacecraft will be stacked together and will travel as a single object. This will allow initial checkout, calibration, and some limited experimentation. During the second stage of operation, the satellites will separate and a simple tether or flexible boom will uncoil, linking the two vehicles. This tethered stage will allow full formation flying experimentation including on-orbit relative position determination and simple closed loop relative position control using the drag panels and microthrusters.

During the final stage of operation, the tether will be cut in order to permit true two-body formation flying for a limited period of time. The tether will have a simple

sub-satellite at its midpoint. Upon ground command, the two halves of the sub-satellite will separate. Each satellite will retain half of the tether and half of the sub-satellite, providing very rough gravity gradient stabilization. [Ref. 11]

d. UW nanosatellite (Dawgstar)

The University of Washington Nanosatellite program is a student run program to design, build and launch the smallest self-propelled satellite (15kg) to be used in a cluster of satellites flown in 2002 as one of the first distributed satellite testbeds in space. UW has university partners (Utah State and Virginia Tech), each of which is designing a satellite to allow the "cluster" testbed. The focus on the UW program has been on distributed control. The sensing will be done using several technologies relating to GPS, and a cross-link system designed by APL-JHU. The actuation will be a set of eight pulsed plasma thrusters, to be used for both attitude and position control. In addition, there are several other important technology developments in this program, including: development of μPPTs for both attitude and orbit/formation control, development of horizon and sun sensors using small, lightweight, CMOS camera technology and distributed ionospheric science. [Ref. 12]

3. Miscellaneous Projects

Project Starshine. The Student Tracked Atmospheric Research Satellite is a small, optically reflective spherical spacecraft. The Naval Research Laboratory in Washington, DC assembled it from eleven hundred sets of aluminum mirror blanks machined by Utah technology students and shipped in kits by project officials to schools around the world where students polished the blanks.

The satellite is 48cm (19in) and was very bright and easily visible to the naked eye. Students recorded their observations online while tracking the satellite. The satellite's orbit decayed at a rate proportional to how much the upper atmosphere was heated by solar activity, thus monitoring sunspots. Starshine was deployed by NASA from a Hitchhiker canister on the Space Shuttle Discovery into a highly inclined low

earth orbit on mission STS-96 in May of 1999, and the satellite re-entered Earth's atmosphere on Feb 18, 2000

Sunsat. Graduate students at the University of Stellenbosch built this South African satellite. It was launched as a piggyback payload on a Delta II from Vandenberg on February 23, 1999. SUNSAT is a micro satellite, weighing 64 kg, with dimensions of 45 cm x 45 cm x 60 cm, with an elliptical polar orbit (620 by 850 km). The satellite holds amateur radio transponders and several other instruments that allow digital store-and-forward capability and a voice 'parrot' repeater that is being used primarily for educational demonstrations. The unit has two VHF and two UHF transmit-receive systems. In addition to amateur radio and school science payloads, Sunsat carries two NASA experiments and an experimental push-broom imager capable of taking pictures of Earth. The high-resolution imager operates in real time on S-band frequencies. Images also can be stored in computer RAM aboard the satellite and then downloaded at lower speeds for retrieval by hams and schools. The participants have made a big effort to use the project to inspire interest in science and engineering in South African high school students.

CubeSat. The CubeSat is a nano-satellite design from Bob Twiggs of the SSDL (Stanford's Space System's Development Laboratory). The motivation is to develop a standard, off-the-shelf-satellite small satellite kit that can be cheaply built, easily adapted for different missions, and launched in clusters to lower the per satellite launch cost. The CubeSat is about 10cm per side and weighs a kilogram (see next page - Fig. 2.5), allowing student groups to be able to build and launch them for around $50k each. Eventually, multiple CubeSats will work together in formation to provide the capabilities of a single large satellite. The company OSSS (One-Stop-Satellite-Solutions) has been formed to commercialize SSDL's CubeSat. Several college teams are now building CubeSats for launch in 2001: CubeSat at Cuesta College Amateur Radio Organization, CubeSat at the University of Tokyo, and Cube-sat at Tokyo Institute of Technology. [Ref. 13]

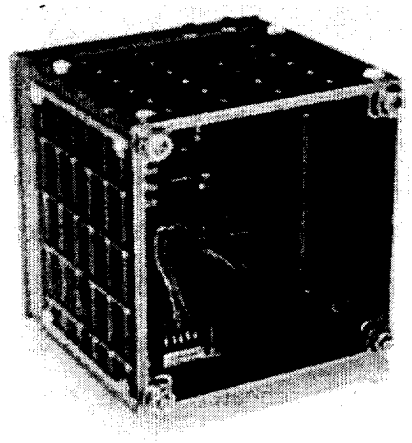

Figure 2.5 Inside a CubeSat (10cm per side)

PANSAT. The Petite Amateur Navy Satellite (PANSAT) is a small satellite designed and built by military officer students, faculty, and staff at the Naval Postgraduate School (NPS). The main objective was to support the Space Systems Engineering and Space Systems Operations curricula by providing a 'hands-on' hardware project where exposure to the many facets of a space system development and life cycle can be experienced. PANSAT further provides educational training while in orbit through a space-based laboratory for officer students at NPS. PANSAT was launched from the Shuttle into a low-Earth orbit on the STS-95 Discovery mission as part of the third International Extreme Ultraviolet Hitchhiker (IEH-3) experiment.

The spacecraft itself provides store-and-forward (packet radio) digital communications using direct sequence spread spectrum modulation. PANSAT operates in the amateur radio 70 cm band with center frequency at 436.5 MHz, a bit rate of 9842 bits per second and 9 MB of message storage. Amateur radio ground stations will be able to utilize PANSAT via a bulletin-board type user interface.

C. CURRENT SYSTEMS AND INDUSTRY LEADERS

1. Aerospace Corp.

In an effort sponsored by Defense Advanced Research Projects Agency (DARPA), Aerospace Corporation scientists and engineers are collaborating with

tockwell Science Center and Stanford University to develop miniature low-cost space latforms to validate microsystems for space applications and advance the development f mass-producible, fully functional nanosatellites (see Fig. 2.6). Aerospace supported reflight activities for an experiment involving two tiny picosatellites to be deployed rom Stanford University's OPAL satellite (see section 2000-present) after its launch by he new Air Force OSPSLV. The picosats were tethered to emulate formation flying vithin the range of low-power radios. A picosat mounted on a 50-meter ground antenna ormed the third element of a rudimentary constellation. MEMS radio-frequency switch rrays were also tested on this mission.

The mission represents one of several programs for systematic testing and use of MEMS in space to be designed and implemented by The Aerospace Corporation. One of he MEMS devices, designed and fabricated at The Aerospace Corporation, comprises an rray of 19 microthrusters that could be used to orient a nanosatellite. Each of the 19 cells epresents a separate thruster like a solid rocket motor on a launch vehicle (see Chapter B for propulsion components).

The mission closed out February 10, 2000 and was the first of a series designed to alidate MEMS technology and demonstrate the capabilities of mass-produced miniature atellites operating in constellations. Another picosat mission was launched July 29, 2000 board the MightySat 2.1 satellite built by the Air Force Research Laboratory (AFRL), nd a third more complex "inspector" mission is planned for 2003.

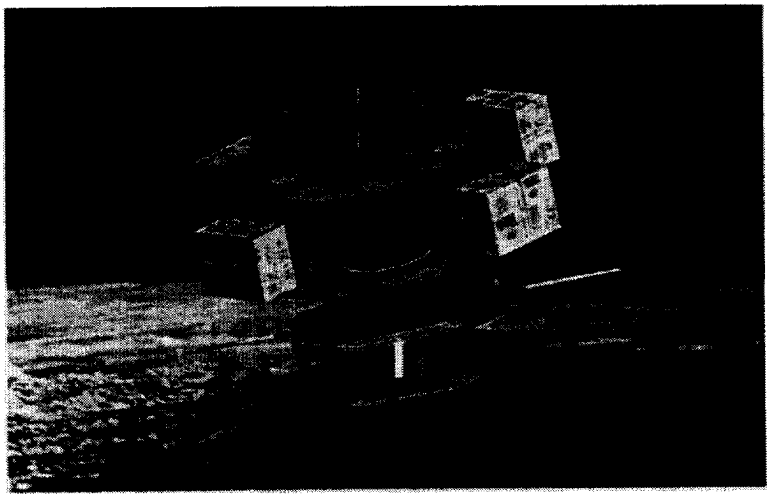

Figure 2.6 Artist Conception of orbiting AEROSPACE Nanosatellite

2. NASA

The Nanosat Constellation Trailblazer mission is the fourth deep space mission in NASA's New Millennium Program. Known as Space Technology 5 (ST-5 for short), the mission will attempt to fly three miniature spacecraft high above the Earth. Each of the spacecraft is about the size of a 'big' birthday cake; 42cm (17 in) across and 20 cm (8 in) high, and weighs about 21.5 kilograms (47 pounds). ST5 will attempt to fly three separate spacecraft in a constellation, performing coordinated movements, communication, and scientific observations as it was a single, larger spacecraft. The payoff from this technology demonstration will enable a series of multi-spacecraft missions in the future. Large numbers of small spacecraft are planned in "constellation class" missions in the next century to perform in-situ measurements of space weather conditions. Space Technology 5 will fly three nanosatellites in a stable major orbit at about 200x 35,790 km altitude.

The spacecraft will be used to test methods for operating a constellation of spacecraft as a single system. The mission will also test eight innovative new technologies in the magnetosphere. The mission is planned for launch in 2003 as a secondary payload on an expendable launch vehicle. The mission is managed by NASA's Goddard Space Flight Center in Greenbelt, Maryland and is budgeted at $28 million.

3. Foreign Universities

The purpose of the Surrey Nanosatellite Applications Program, by Surrey Satellite Technology Ltd (SSTL) located at Surrey University, is to develop practical, modular, multi-mission satellite buses within mass ranges of 1-10 kg, and to demonstrate the use of miniature electrical and mechanical COTS technologies in space. It also is to provide vehicles for the education and training of students in spacecraft engineering at the undergraduate and post-graduate level. The first accomplishment of this was by the development of the ultra-low-cost demonstration spacecraft ('SNAP-1' – see above 2000-

present) within a year, by a team comprising undergraduates, Masters and Ph.D. students, with the supporting expertise from SSTL and CSER staff.

Additionally, MicroStructure Technology (MST) at Uppsala University in Sweden will launch in a few years the first European nanosatellite. Researchers within the Center for Advanced Micro Engineering (AME) are contributing on microsystems research hoping to increase the European nanosatellite knowledge base. A nanosatellite project has been initiated at AME to promote system oriented research work.

D. NANOSATELLITES FLYING TOGETHER

One distinctive concept, which demonstrates the unique capabilities of nanotechnology and many of the above small satellite designs, is formation flying. The next chapter's thrust will be to present how to use these smaller nanosatellites in numerous formations. Many concepts have started to surface on what types of formations are better at certain missions, and cluster lifetime orbit analysis simulations are quickly narrowing down the required fuel expense and attitude control needed to maintain the formation dynamics.

THIS PAGE INTENTIONALLY LEFT BLANK

III. NANOSATELLITE FORMATION DYNAMICS

A. INTRODUCTION

In recent years, the innovative idea of distributing the functionality of current larger satellites among smaller, cooperative satellites has been sincerely considered for various space missions to achieve goals that are not possible or very difficult to accomplish with a single satellite. For instance, one possible use for nanosatellites is clusters of satellites flying together in formation for high-resolution, synthetic-aperture imaging. In this case, groups of nanosatellites are operated cooperatively to act as a sparse aperture with an effective dimension larger than can be achieved by a single, larger satellite. The system adds flexibility since the formation and therefore aperture size and orientation are adjustable on orbit. [Ref. 14] Flying many satellites in formation presents flexibility to mission designers given that the individual satellites will be capable of repositioning themselves with respect to each other to achieve diverse tasks. By accurately computing the preliminary Keplerian orbit elements, the satellites can realize the desired close separation and cluster orientation desired to operate the necessary missions.

In particular, NASA and U.S. Air Force have identified multiple spacecraft formation flying (MSFF) as an enabling technology for future missions. [Ref 15] Another buzzword denoting this division of labor among smaller satellites is becoming referred to as Distributed Satellite Systems (DSS) in DoD, NASA and the commercial sectors. NASA's Mission to Planet Earth and New Millennium programs have acknowledged the benefits of satellite formation flying and have incorporated an enhanced formation flying experimentation in the Earth Observing System mission. [Ref. 16] The European Space Agency has engineered a sophisticated formation for its Cluster mission to study the Earth's magnetosphere, the Orion program is intended for a low cost display of GPS uses in formation flying, and the Laser Interferometer Space Antenna (LISA) mission is a heliocentric formation-flying mission intended to identify gravity waves. The US Air Force Research Laboratory's TechSat 21 program is a technology demonstration of the

'virtual satellite' concept. [Ref. 17] The TechSat 21 program was reviewed in Section II (above).

Advances in miniaturization using MEMS technology leads to estimation of nanosatellites masses of less than 1 kg. In some instances, simple satellites-on-a-chip may have a mass of order 10^{-3} kg (picosats). A particular original concept is the use of large numbers of such nanosatellites/picosatellites to shape constellations to permit the real-time acquisition of distributed information. For example, a spherical constellation of nanosatellites has been proposed to provide a real-time, three-dimensional view of the magnetosphere. Each nanosatellite can be thought of as a 'pixel' of a three-dimensional data set. To supply high-quality spatial and temporal resolution for such a mission, large numbers of nanosatellites are necessary. Because these ultra-low mass satellites can be passive sensors without active orbit control, environmental effects such as air drag will form the evolution of the constellation. For MEMS fabricated nanosatellites, with a mass of order 0.1 kg or less, constellations could include several thousand elements.

Other concepts have envisioned large numbers ($>10^3$) of nanosatellites to be deployed from a dispenser to provide a continuous planar ring of satellites for communication purposes. Such constellations would be fashioned by dispensing nanosatellites over a range of orbit radii at the identical inclination to induce differential azimuthal motion, therefore forming a homogeneous ring. With a large number of satellites in basically random azimuthal locations, communication links grow to be robust for on-orbit failures. Furthermore, the constellation is short lived because air drag will eventually remove all the nanosatellites. Such concepts are attractive for military communications, where the constellation is positioned from a single launch vehicle and formed to sustain a dedicated remote operation. A related concept requires clusters of nanosatellites to be launched into random orbits to piggyback launches on any available vehicle. Analysis shows that 400 nanosatellites can provide ~95% coverage of the globe. [Ref. 18] The constellation would require the continual deposition of new nanosatellites to make up for losses from on-orbit failures and air drag removal.

Formation flying clusters of satellites also provide for graceful degradation of performance during times of satellite failure. If a single large satellite has a system

failure, the entire mission is at risk. If a single satellite in a cluster fails, the remaining satellites in the cluster may maintain mission objectives at a lower performance level. The cluster could then be brought back up to mission design specifications or even improved with the addition of another inexpensive replacement satellite.

The following chapter investigates several satellite formation-flying designs, with particular emphasis on the projected circular formation. These cluster formations are described with regard to their basic orbital equations of motion and then are populated through computation from a technique derived from the Aerospace Corporation. [Ref. 19] A MATLAB program was written that determined both the mothersat and eight remotes' position and velocity vectors, which were in turn entered into STK. This basic formation simulation provides an initial look into the orbital dynamics and a brief look into perturbations that affect a LEO cluster with the ΔV required to maintain that cluster.

B. INITIAL EQUATIONS OF MOTION OF SATELLITE FORMATIONS

Satellite formations that are optimal for Interferometric Earth imaging are discussed in AIAA paper 98-4379, *Optimization of Geosynchronous Satellite Constellations for Interferometric Earth Imaging* [Ref. 20], and in the following sections four satellite formations (in-plane, in-track, circular, projected circular) are obtained for a variety of satellite applications. The desired trajectories are carefully designed natural orbits so that the energy costs to fly along these trajectories is minimized.

Satellite formation flying designs can be derived from the linearized equations of relative motion for two objects under the influence of a point mass gravitational field. These equations are commonly known as Hill's equations. From Vallado's text [Ref. 21], a detailed derivation of Hills's equation is presented, which take the following form for unperturbed motion:

$$\begin{aligned} \ddot{x} - 2\omega\dot{y} - 3\omega^2 x &= 0 \\ \ddot{y} + 2\omega\dot{x} &= 0 \\ \ddot{z} + \omega^2 z &= 0 \end{aligned} \tag{3.1}$$

Here, x is the radial difference between the two objects, y is the along-track difference, z is the cross-track difference (see Fig. 3.1 below), and ω is the mean motion of the reference object.

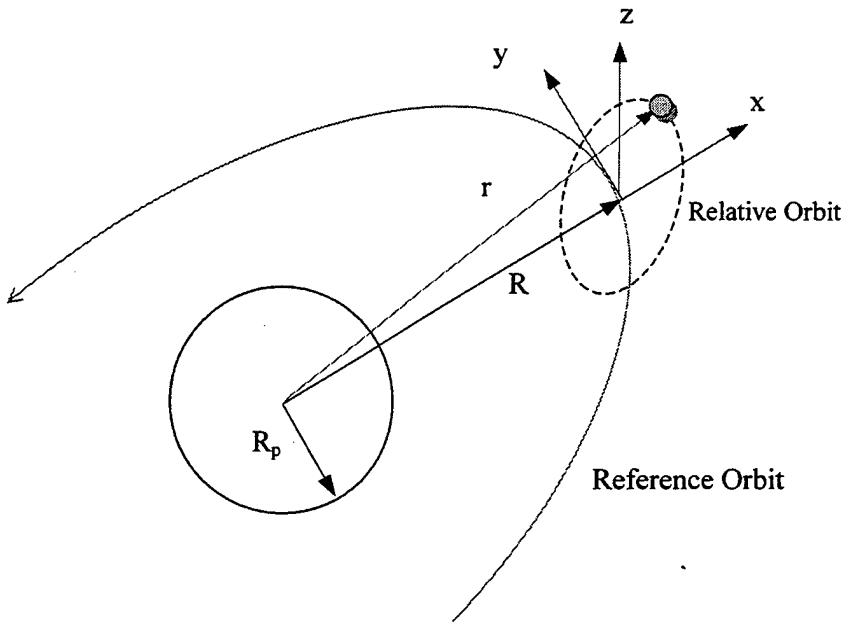

Figure 3.1 Hill's reference frame for satellite relative motion.

The unperturbed version of Hill's equations can be solved analytically, with the solution being:

$$x(t) = \frac{\dot{x}_0}{\omega}\sin(\omega t) + (3x_0 + \frac{2\dot{y}_0}{\omega})\cos(\omega t) + (4x_0 + \frac{2\dot{y}_0}{\omega})$$

$$y(t) = \frac{2\dot{x}_0}{\omega}\cos(\omega t) + (6x_0 + \frac{4\dot{y}_0}{\omega})\sin(\omega t) - (6\omega x_0 + 3\dot{y}_0)t - \frac{2\dot{x}_0}{\omega} + y_o \qquad (3.2)$$

$$z(t) = \frac{\dot{z}_0}{\omega}\sin(\omega t) + z_0\cos(\omega t)$$

In order to avoid secular, or long-term, growth in the relative motion, Eq. (3.2) needs a constraint on its secular term to be set to zero:

$$\dot{y}_0 = -2x_0\omega \qquad (3.3)$$

It can then be shown that this constraint results in a displaced orbit with the same energy, and thus the same semi-major axis, as the reference orbit through first order in the small displacements. By enforcing the constraint, Hill's equations become:

$$x(t) = \frac{\dot{x}_0}{\omega}\sin(\omega t) + x_0\cos(\omega t)$$

$$y(t) = \frac{2\dot{x}_0}{\omega}\cos(\omega t) - 2x_0\sin(\omega t) - \frac{2\dot{x}_0}{\omega} + y_0 \qquad (3.4)$$

$$z(t) = \frac{\dot{z}_0}{\omega}\sin(\omega t) + z_0\cos(\omega t)$$

where terms with '0' subscripts refer to initial conditions. These equations provide for formation flying design.

In the above equations, it can be seen that the radial (x) and along-track (y) components of motion are uncoupled from the cross-track (z) component of the relative motion. The motion in the radial/along-track plane can be shown to be an ellipse of fixed eccentricity ($e = 0.866$) with an arbitrary along-track offset. All unperturbed formation flying designs must project this elliptical motion into the radial/along-track plane.

In the linearized model, the cross-track (z) component of the relative motion is a simple harmonic oscillator. Combining the elliptical motion in the radial/along-track direction with the oscillatory motion in the cross-track direction yields the family of ellipses that describe all formation-flying designs. [Ref. 14]

Six initial conditions must be specified in the solutions to Hill's equations. These initial conditions can be thought of as Cartesian or Keplerian element differences between the two satellites and allow for six constraints or design parameters to be placed on the formation. One constraint was specified when the secular terms were removed from the solution to Hill's equations (see Eq. (3.3) above). This can be thought of as requiring the semimajor axis of the two satellites to be equal. Another constraint is the offset of the elliptical motion in the radial/along-track plane, y_0. This leaves four design parameters, which describe the size, eccentricity, orientation, and initial location in the ellipse of relative motion. These also can be thought of as the size of the ellipse in the

radial/along-track plane, the initial location within that ellipse, the amplitude of the oscillation in the cross-track plane, and the initial location in the cross-track oscillation.

1. Basic Remote Motion in the Formation

The remote formation, as mentioned above, is derived from Hill's equations. The center of the formation is a satellite flying in a circular orbit, defined as 'mothersat', which then has a moving frame attached to it. Its x and y directions are shown in Fig. 3.2

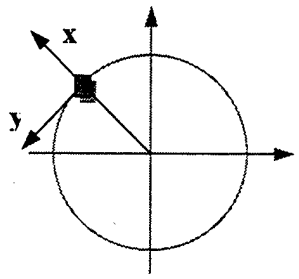

Figure 3.2 Moving Frame

The z direction is pointing upward orthogonal to both the x and y axes. Under this coordinate system, the dynamic equations of a remote, 'Sat2', are:

$$\ddot{x} - 2\omega\dot{y} - \omega^2(r_0 + x)\{1 - r_0^3[(r_0 + x)^2 + y^2 + z^2]^{-3/2}\} = v_1$$

$$\ddot{y} + 2\omega\dot{x} - \omega^2 y\{1 - r_0[(r_0 + x)^2 + y^2 + z^2]^{-3/2}\} = v_2 \qquad (3.5)$$

$$\ddot{z} + \omega^2 r_0^3 z[(r_0 + x)^2 + y^2 + z^2]^{-3/2} = v_3$$

Under the moving frame, the desired trajectory of Sat2 in the circular formation satisfies:

$$x_d(t) = (\dot{x}_0 / \omega)\sin(\omega t) + x_0\cos(wt)$$

$$y_d(t) = (2\dot{x}_0 / \omega)\cos(\omega t) - 2x_0\sin(wt) \qquad (3.6)$$

$$z_d(t) = \sqrt{3}(\dot{x}_0 / \omega)\sin(\omega t) + \sqrt{3}x_0\cos(wt)$$

The desired path is a nonthrust trajectory for the linearized dynamics of Eq. (3.5). The free variables, x_0 and $\dot{x}_0$ are the initial value of x and the derivative of x. In the inertially fixed frame, the path is:

$$r = 2\sqrt{\dot{x}_0^2/\omega^2 + x_0^2} \tag{3.7}$$

All formation designs that follow will be constrained to these equations of motion of the remotes (Sat2s). As will be seen, most parts of these equations can be canceled out, or simplified.

2. In-Plane Formation

The in-plane formation is the simplest of all cluster designs. It consists of a group of satellites occupying the same orbital plane and separated by mean anomaly. In Hill's equations, setting all initial conditions, except for y_0, to zero, represents this formation. The solutions are then:

$$\begin{aligned} x(t) &= 0 \\ y(t) &= y_0 \\ z(t) &= 0 \end{aligned} \tag{3.8}$$

where y_0 represents the amount of in-plane spacing between two satellites. This can be related to the mean anomaly separation by:

$$\Delta M = \frac{y_0}{a} \tag{3.9}$$

where ΔM is the mean anomaly separation and a is the semimajor axis of the orbits. Again, this formulation being based on Hill's equations assumes that the orbits are circular, are at least nearly so. The primary advantage of the in-plane formation is its simplicity in design, deployment and control.

3. In-Track Formation

The in-track cluster design is a special case of the in-plane formation. Here the satellites all share the same ground track. To do so, the satellites have to occupy slightly different orbital planes separated by right ascension of the ascending node (Ω), which accounts for the rotation of the earth. The difference in the equations can be seen by the addition of a cross-track oscillation that represents the difference in right ascension of the ascending node. The solutions to Hill's equations are then:

$$x(t) = 0$$

$$y(t) = y_0 \tag{3.10}$$

$$z(t) = \frac{\omega_e}{\omega}\sin(i) y_0 \cos(\omega t)$$

where y_0 represents the amount of in-plane spacing between two satellites, ω is the mean motion of the orbits, i is the inclination of the orbits, and ω_e is the rotation rate of the Earth. The trailing satellite is behind the lead by some difference in mean anomaly; relate this difference in mean anomaly to a difference in time (i.e. Δt). Then calculate the nodal difference $\Delta\Omega$ such that the second satellite is over the same point as the lead satellite at some time in the future ($t + \Delta t$). The equations take the following form:

$$\Delta M = \frac{y_0}{a}$$

$$\Delta t = -\frac{\Delta M}{\omega} = -\frac{y_0}{a\omega} \tag{3.11}$$

$$\Delta\Omega = \omega_e \Delta t = -\omega_e \frac{y_0}{a\omega} = \frac{z_0}{a\sin(i)}$$

$$z_0 = -\frac{\omega_e}{\omega}\sin(i) y_0$$

where ΔM is the mean anomaly separation and $\Delta\Omega$ is the nodal separation. The attractiveness of the in-track formation is that each satellite in the formation passes over the same exact spots on the ground, which is valuable for Earth sensing missions. An example screenshot from STK for an in-track formation is shown in Appendix 3.1.

4. Circular Formation

The circular formation is one in which satellites maintain a constant distance from each other. It can be derived from Hill's equations analytically or geometrically. The analytic approach takes the solutions to Hill's equations and determines relations between the initial conditions given the constraint:

$$x^2 + y^2 + z^2 = r^2 \tag{3.12}$$

where r is the radius of the formation. The geometric approach takes advantage of the fact that the relative motion in the radial/along-track planes (x/y) is fixed in eccentricity. From either approach, the following relations are found:

$$\begin{aligned} y_0 &= \frac{2}{\omega}\dot{x}_0 \\ \dot{y}_0 &= -2\omega x_0 \\ z_0 &= \pm\sqrt{3}x_0 \\ \dot{z}_0 &= \pm\sqrt{3}\dot{x}_0 \end{aligned} \tag{3.13}$$

where the first two conditions set the along-track offset and drift to zero. These constraints show that there are two planes in which the circular formation is possible. Both intersect the cross-track/along-track plane along the along-track axis but one is inclined 30° to that plane and the other is inclined at −30°. If the 30° case is chosen, the following solutions to Hill's equations are found:

$$x(t) = \frac{\dot{x}_0}{\omega}\sin(\omega t) + x_0\cos(\omega t)$$

$$y(t) = \frac{2\dot{x}_0}{\omega}\cos(\omega t) - 2x_0\sin(\omega t) \tag{3.14}$$

$$z(t) = \sqrt{3}\frac{\dot{x}_0}{\omega}\sin(\omega t) + \sqrt{3}x_0\cos(\omega t)$$

Note that the formation design again has two free parameters: x_0 and $\dot{x}_0$. These free parameters specify the radius and phasing of one satellite in its circular path about the reference satellite. The four other initial conditions were constrained for eliminating along-track drift, eliminating the along-track offset, and setting the eccentricity and orientation of the ellipse of relative motion.

If the initial conditions of the solutions to Hill's equations presented in Eq. (3.14) are formulated in terms of the cluster radius and phasing, the following equations arise:

$$x_0 = \frac{r}{\sqrt{3\tan^2(\theta)+4}}$$

$$\dot{x}_0 = \frac{r\omega}{2}\frac{\sqrt{3\tan^2(\theta)}}{\sqrt{3\tan^2(\theta)+4}} \tag{3.15}$$

where r is the radius of the formation, and θ is the phase angle of the satellite measured clockwise from the cross-track(z) direction.

From Equation (3.14)/(3.15), given a circular-reference orbit and desired cluster radius and phasing, it is possible to convert the reference elements from Keplerian to Cartesian, after coordinate transformations add the Cartesian differences to get the position and velocity vectors of the satellites in the circular clusters, and then convert the Cartesian elements back to Keplerian for all the satellites in the cluster.

The Keplerian element differences for a circular formation are highly dependent on the phasing and initial conditions of the reference orbit. For two arbitrary points in the cluster, there will be differences in inclination (i), right ascension of the ascending node

(Ω), argument of perigee (w), and mean anomaly (M). Generally, satellites in a cluster will have the same eccentricity except in the case where the reference orbit is not circular. There are conditions, however, where two satellites in the cluster can have the same inclination or right ascension of the ascending node.

The circular formation has two properties which make it attractive: 1) the satellites maintain a constant distance from each other, enabling precise measurements for use in missions such as interferometry, and 2) unlike the in-plane and in-track formations, the circular cluster presents a two dimensional array, increasing dimensional resolution for imaging, geolocation potential, and numerous other missions. An example screenshot from STK for a circular formation with four remotes is shown in Appendix 3.1.

5. Projected Circular Formation

The projected circular formation is very close in design to the circular formation. This formation will be covered briefly here in this section, and in more detail with another example of equation setup in Section D (satellite formations with constant apparent distribution – *see below*).

The difference is that the projected circular cluster only maintains a fixed distance in the along-track/cross-track (y/z) plane. Another way to describe the projected circular formation is to say that when the ellipse of relative motion is projected onto the along-track/cross-track plane, it produces a circle. This results in the following constraint:

$$y^2 + z^2 = r^2 \tag{3.16}$$

where r is the radius of the projected circle.

Like the circular cluster, the constraint can be applied to the initial conditions to the solutions of Hill's equations to produce:

$$y_0 = \frac{2}{\omega}\dot{x}_0$$

$$\dot{y}_0 = -2\omega x_0$$

$$z_0 = \pm 2x_0 \tag{3.17}$$

$$\dot{z}_0 = \pm 2\dot{x}_0$$

where the first two conditions set the along-track drift and offset to zero. There are two planes in which the projected circular formation is possible. Both intersect the cross-track/along-track plane along the along-track axis but one is inclined 26.565° to that plane and the other is inclined at −26.565°.

If the 26.565° case is chosen, the following solutions to Hill's equations are found:

$$x(t) = \frac{\dot{x}_0}{\omega}\sin(\omega t) + x_0\cos(\omega t)$$

$$y(t) = \frac{2\dot{x}_0}{\omega}\cos(\omega t) - 2x_0\sin(\omega t) \tag{3.18}$$

$$z(t) = \frac{2\dot{x}_0}{\omega}\sin(\omega t) + 2x_0\cos(\omega t)$$

The formation design again has the same two free parameters, which represent the radius and phasing of projected circular path.

If the initial conditions of the solutions to Hill's equations in Eq. (3.17) are formulated in terms of the cluster radius and phasing, the following arise:

$$x_0 = \frac{r}{2}\cos(\theta)$$

$$\dot{x}_0 = \frac{r\omega}{2}\sin(\theta) \tag{3.19}$$

Like the circular formation design, the Keplerian element differences show up in inclination, right ascension of the ascending node, argument of perigee, and mean anomaly, and the variations are dependent on the reference orbit and phasing. The primary advantage of the projected circular cluster over the circular cluster is that a fixed distance separates the satellites when the formation is projected onto the along-track/cross-track plane. This has applications for ground observing missions.

C. REMOTE CLUSTERS WITH CONSTANT APPARENT DISTRIBUTION

The work presented in this section continues the work started at the end of the last one - the problem of creating a cluster of satellites that would maintain a constant, or nearly constant, shape and size when viewed from the Earth. Such a cluster would seem to have a constant apparent (as opposed to physical) distribution. In such a formation, all satellites would have a clear field of view of the surface, and would remain in sufficiently close formation to share their information. Such formations are of interest for large distributed-aperture sensing, for example. Another possibility is that of forming clusters from many small, inexpensive satellites, each with a particular type of sensor and some computing power. Remaining in a close formation would allow the satellites to share information and computing ability among themselves.

For such missions, it might be unnecessary to maintain extremely precise relative positions. It might be sufficient to know the relative position accurately, and to remain in close enough proximity to allow intersatellite communication. In addition, an effect of constant apparent distribution is that the angular dispositions of the satellites relative to their ground targets and each other would be constant.

Since it has been mentioned that one of the desires of nanosatellite designs is to reduce the need for station-keeping thrust, orbits in which the natural motion of the satellites keeps them in a cluster are required. The need for station keeping would then be reduced to eliminating the effects of perturbations on the array (covered below in Section E). These effects will be found in the bulk motion of the array and in the relative motions of the satellites in the array. For missions in which precise knowledge of position is the

primary goal, some cyclic perturbations may be acceptable if they are sufficiently small and well understood.

1. Problem Description

In what follows, the motion of a satellite will be described with respect both to a moving reference point and as seen by an observer on the surface of a spherical planet. The motion of the reference point can be visualized by thinking of it as the position of a (possibly hypothetical) reference satellite on a circular orbit of radius R, which will be referred to as the reference orbit. This reference point will serve as the origin of a local coordinate system. This reference frame was first described by Hill, who derived it in his work on the motion of the moon about the Earth.

Let $\boldsymbol{R}$ be the position of the reference satellite (mothersat), following the reference orbit under idealized two-body motion, and $\boldsymbol{r}$ the position of a nearby point (the remote). Both $\boldsymbol{R}$ and $\boldsymbol{r}$ are expressed in an inertial frame centered at the planetary center of mass. Hill's coordinate frame moves with the reference point, and rotates such that the *x-axis* is aligned with $\boldsymbol{R}$. The *y-axis* is tangent to the reference orbit at the reference point, and positive in the direction of the orbital motion. The *z-axis* completes the orthogonal set, as was illustrated earlier in Fig. 3.1. Thus, the reference point is also the origin of the moving reference frame.

Hill's frame allows the motion of the actual satellite to be described with respect to the reference point. It will be shown that the motion of the satellite in this frame will create an orbit; this orbit will be called the relative orbit, as shown in Fig. 3.3 below (passing through the plane at some arbitrary angle). The primary interest however, is in the relative motion as it appears to a fictional observer on the planetary surface, whose position is always on the ray connecting the center of the planet to the reference point. This observer represents the point on the surface that is the subject of observation by the satellite cluster.

The concept of an apparent orbit now can be defined. Consider a point on the planetary surface that moves with time such that it is always between the center of the

planet and the origin of Hill's frame. The apparent orbit is the motion of the satellite relative to the reference point as seen from this point. As this is purely a matter of the line of sight from the viewer to the satellite, there is no physical meaning to the apparent orbit. However, it is helpful to visualize it as the trace left by the intersection of the line of sight as it passes through the y - z plane in the Hill's coordinate frame, as shown in Fig. 3.3.

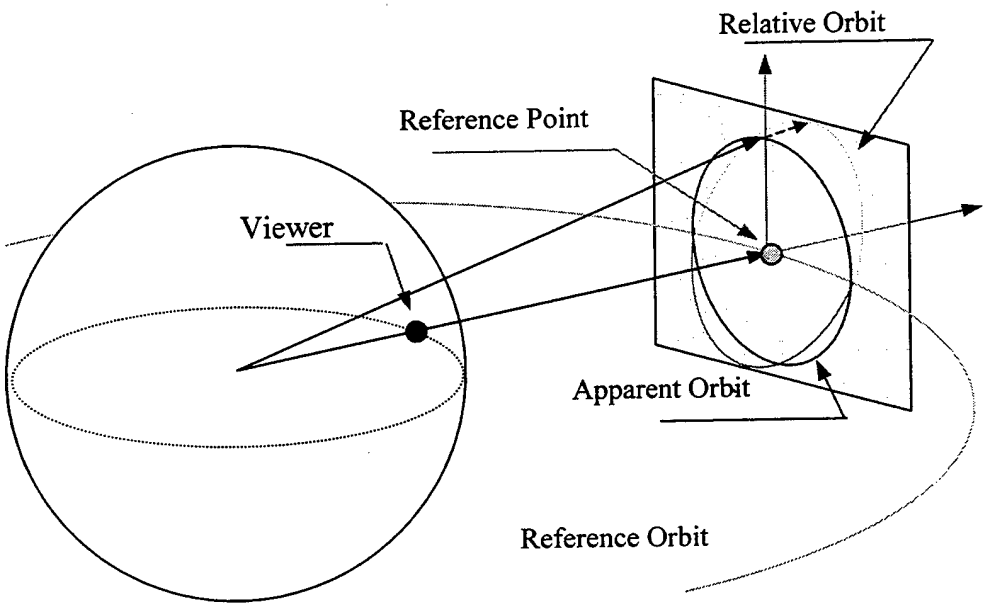

Figure 3.3 Reference, relative, and apparent orbits

The analysis that follows will be primarily concerned with three angles that describe the position of the satellite on the apparent orbit. The elevation angle κ, the lateral angle λ, and the rotary angle ϕ are shown in Fig. 3.4. The angles are all positive as shown, with ϕ increasing in right-hand rotation about the Hill's-frame *x-axis*.

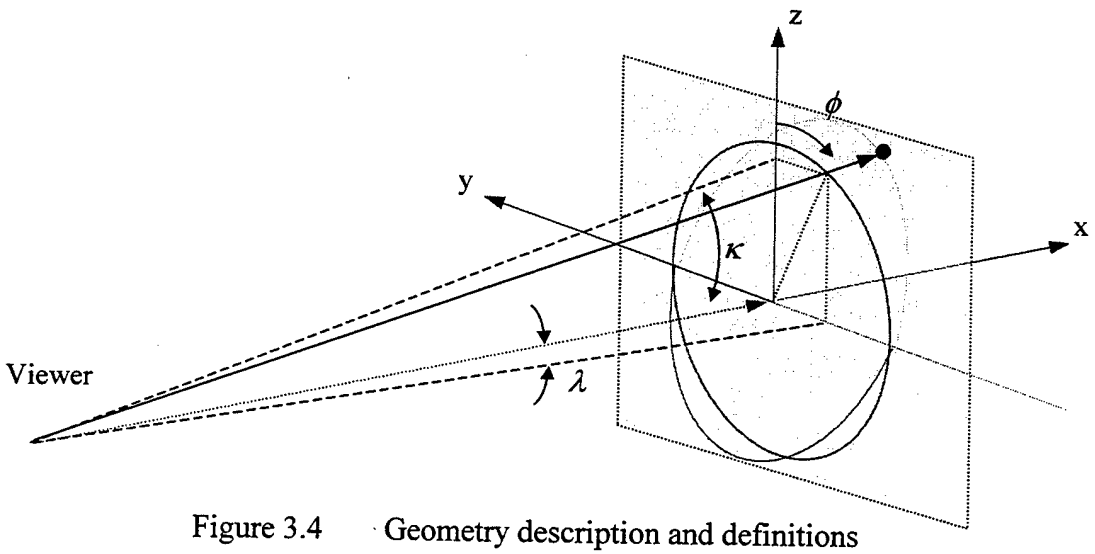

Figure 3.4 Geometry description and definitions

The maximum value of λ will be referred to as the angular width of the orbit, and the maximum value of κ as the angular height. R_P will denote the radius of the planet, and the value $R - R_P$ will be called the altitude of the reference orbit. This is also the mean altitude of the satellite cluster.

Using this definition, a perfectly circular apparent orbit would result in a constant total angle between the line of sight and the line joining the viewpoint to the origin of the Hill's frame. The apparent orbit can then be calculated by multiplying the angles by $R - R_P$. The difference in this formal method and the visualization suggested above is extremely small for clusters in which the cluster radius is small with respect to its mean altitude.

The symbols a and e will denote the semimajor axis and eccentricity of an orbit. The variable ω is the mean motion or average angular motion of a body on an orbit, and for an elliptic orbit is given by the relation $\omega = \sqrt{\mu / a^3}$, where μ is the gravitational parameter of the central body (the mass of the planet times the universal gravitational constant). The true anomaly (v) of a point on an eccentric orbit will be measured from periapsis, as shown in Fig. 3.5. In this case, the reference plane will be the plane of the circular orbit, and the line of nodes will be taken to be the line of intersection of the two orbit planes. The argument of periapsis (w) of the eccentric orbit will be measured from this line of nodes. The inclination will be denoted i and will be the angle between the two

orbit planes. Finally, the angle $u = w + v$ is the angle from the line of nodes to the radial vector. Note that this is defined for circular as well as eccentric orbits.

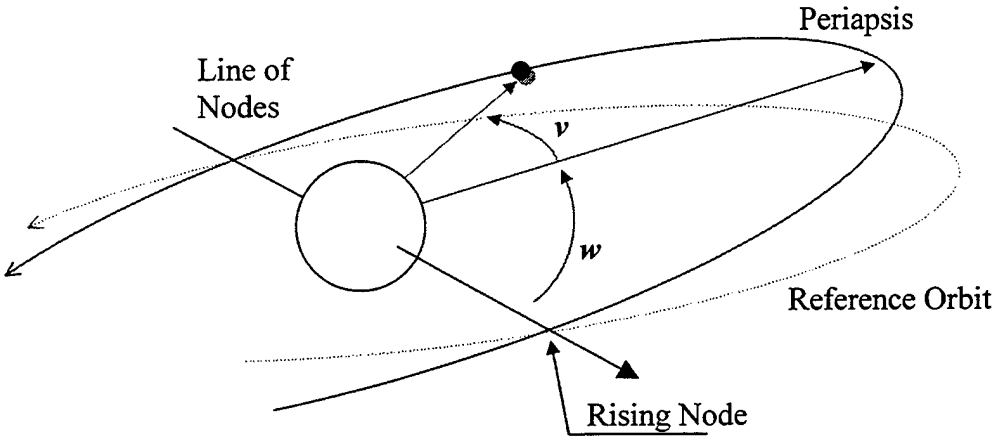

Figure 3.5 Orbital elements of the eccentric orbit.

2. Linearized Approach

The Clossey – Wiltshire (C–W) equations is an accepted choice for describing the motion of a satellite near a circular reference orbit [Ref 21]. They are defined in Hill's reference frame as in Fig. 3.1, and are generally referred to as Hill's equations. Remember (from Section B) the equations are written:

$$\ddot{x} - 2\omega\dot{y} - 3\omega^2 x = 0$$

$$\ddot{y} + 2\omega\dot{x} = 0 \qquad (3.1)$$

$$\ddot{z} + \omega^2 z = 0$$

It follows that the out-of-plane motion is given by:

$$z(t) = A_z \cos(\omega t + \phi_z) \qquad (3.20)$$

where A_z is the magnitude and ϕ_z is a constant phase shift. Solving for x and y is only slightly more difficult. Following usual practice, integrate y to get:

$$\dot{y} = -2\omega x + k \qquad (3.21)$$

where k is a constant of integration. Substitute this into the x equation to get:

$$\ddot{x} = -\omega^2 x + 2\omega k \tag{3.22}$$

This is directly solved to get:

$$x(t) = A_x \cos(\omega t + \phi_x) + 2k/\omega \tag{3.23}$$

which is substituted into Eq. (3.1) and integrated to get:

$$y(t) = -2A_x \sin(\omega t + \phi_x) - 3kt + c \tag{3.24}$$

where c is the constant of integration.

Because a purely cyclic motion is requires with the same period as the reference orbit for this method, $k = 0$; c is simply an offset term and can be given the value zero without loss of generality.

Only the orbit as it appears from the surface of the planet is what is being focused upon. In keeping with the assumptions made to linearize the equations of motion, the assumption is made that the variation in r is negligible with respect to the altitude of the orbit The appearance of the orbit will then be its projection on the y - z plane. This shows:

$$\begin{aligned} y(t) &= -2A_x \sin(\omega t + \phi_x) \\ z(t) &= A_z \cos(\omega t + \phi_z) \end{aligned} \tag{3.25}$$

Setting $\phi_x = \phi_z$ results in a perfectly elliptic projection. By properly specifying the initial conditions, it is possible to set $A_z = 2A_x$ and the apparent orbit becomes a circle. Setting $\phi_x = \phi_z + \pi$ also results in an elliptic projection, however the direction of the projected motion will be reversed. The statement that the apparent orbit is the y-z projection assumes that the viewpoint is on the line connecting the center of the planet to the center of the relative orbit.

Because the initial angle ϕ_z in Eqn. (3.25) is arbitrary, it is possible to place as many satellites in a circular apparent orbit as desired, each separated from the next by some constant angle. This would give a "pinwheel" effect from the planetary surface as

the satellites rotate about the center of the cluster. The cluster would spin about its own center once during each orbit of the planet.

The radius of the apparent orbit is also arbitrary. Thus, it is possible to create a cluster of an almost arbitrary number of satellites, by creating concentric rings about the reference satellite, as in Fig. 3.6. The period of the apparent orbit is always that of the reference orbit, so that the entire cluster will maintain its shape relative to the center. Thus, separation angles such as ϕ_{12} in Fig. 3.6 should remain constant.

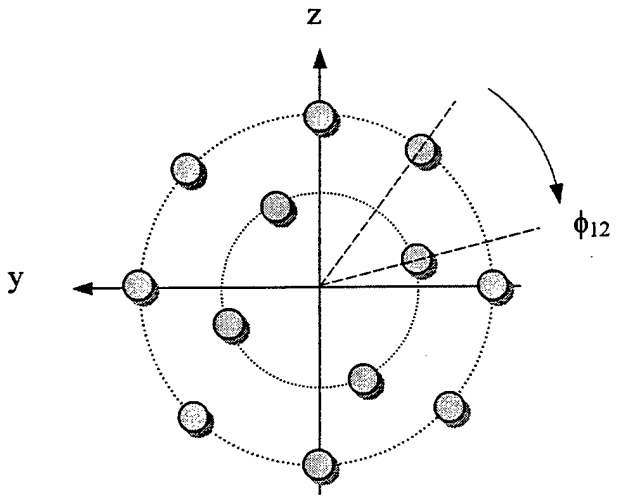

Figure 3.6 Apparently circular cluster of satellites.

As the C–W equations are linearizations, it is to be expected that they do not fully describe the relative motion of the satellite. Examining the higher-order terms in the orbital equations can make an approximation of their error. This is the subject of the next section.

The height of the apparent orbit can be shown to be independent of the width. Thus, this technique can also be used to generate a relative orbit that is very nearly circular in actuality, and which appears elliptic when viewed from the planetary surface.

3. Orbital Mechanics

The motion of the satellite described by the C–W equations is caused by slight differences in the orbital parameters of the satellites. The satellite in the elliptic orbit

moves more slowly than the reference when at apoapsis, and more quickly near periapsis. It thus seems to lag behind and then to catch up. When combined with inclination, this leads to an apparent orbit about the reference satellite.

Investigating the apparent orbit in terms of the orbital elements is not as straight forward as using the linear equations, but this approach allows an investigation of the limits of the linearized approach, and an estimate of the corrections due to nonlinearity. In this section, the eccentricity and inclination parameters required to produce a circular apparent orbit will be investigated.

In developing the ideas of this section, attention will be confined to orbits in which periapsis is 90° from the line of nodes. This ensures the symmetry of the apparent orbit about the Hill's-frame z-axis. (Recall that the line of nodes as defined here will be the line of intersection of the orbital plane with the reference plane.)

The description of the apparent orbit will be expressed in terms of the eccentricity of the satellite orbit. These terms will be on the order of e; thus, second-order terms in e may be considered first-order corrections. In the following analysis, estimates for these correction terms will be found.

a. Apparent Angular Width

The needed eccentricity is first examined to produce an apparent orbit of a particular width. The width will be defined by projecting the line of sight to the satellite onto the reference plane. The angle between this projection and the line of sight to the reference point is then the angular separation of the satellite and the reference point (this is the angle λ in Fig. 3.4). The width of the orbit is then the maximum value of this angle.

If the inclination of the orbit is zero, the angle is easily computed, taking the reference orbit and the eccentric orbit to have equal semimajor axes and thus equal periods. The motion of the reference point is then equivalent to the mean motion of the eccentric orbit. The separation at any point is then the difference between the true anomaly v and the mean anomaly M. Assuming the inclination is small enough that its

effects are negligible then allows extraction of some information. The expansion as given in Vallado [Ref. 21] is:

$$v - M = 2e\sin M + \tfrac{5}{4}e^2 \sin 2M + \ldots \tag{3.26}$$

Finding the maximum, taking the expansion through second order, and taking the derivative with respect to M results in:

$$4e\cos M + 5e^2 \cos 2M = 0 \tag{3.27}$$

For $e \rightarrow 0$, this leads to values of M approaching $\pi/2$. Setting $M = \pi/2 + \delta$ and dividing through by e allows Eq. (3.27) to be rewritten as:

$$-2\sin\delta - 5e\cos 2\delta = 0 \tag{3.28}$$

Again, $e = 0$ gives $\delta = 0$, and for very small e, have δ is approximately $-5e/2$. The sign of δ is less important than the knowledge that δ is of order e.

Using these results, Eq. (3.26) can now be written:

$$v - M = 2e\sin\delta - \tfrac{5}{4}e^2 \sin 2\delta + \ldots \tag{3.29}$$

Because δ is small, $\cos\delta \sim 1$ and $\sin 2\delta \sim 2\delta$. Because δ is of order e, the second term on the right in the above equation is $\sim e^3$ and can be ignored. Thus, to second order:

$$v - M = 2e \tag{3.30}$$

Thus, the angular width of the apparent orbit as seen from the center of the central body is $4e$. From the surface of the planet, the angular spread is wider. Letting λ denote the angle between the lines of sight to the satellite and to the reference, geometry gives:

$$\lambda = \tan^{-1}\left(\frac{r\sin(v-M)}{r\cos(v-M) - R_p}\right) \tag{3.31}$$

Expanding the radius of the elliptic orbit in M and e, again writing M as $\pi/2 + \delta$, gives:

$$r = R[1 - e\sin\delta + (e^2/2)(\cos 2\delta - 1) + \ldots] \tag{3.32}$$

Using the expansions for v - M and r as expanded, the first order approximation is:

$$\lambda = \frac{2R\cos\delta}{R - R_p} e \approx \frac{2R \cdot e}{R - R_p} \tag{3.33}$$

and that the coefficient of the second-order term is of order δ, making the term of third order. This gives a total angular width of the apparent orbit of:

$$2\lambda \approx 4e[R/(R - R_p)] \tag{3.34}$$

For a low-altitude orbit, R_P may be nearly as large as R, and thus the angular spread of the apparent orbit as seen from the planetary surface might be several times larger than the value of v - M.

b. Correction for Inclination

To allow for orbital inclination, the expansions used to compute the width of the apparent orbit must be extended to include the inclination. Consider the angle between the projection of the radial vector onto the reference plane and the projection of the eccentricity vector (that is, the vector from the center of the planet to periapsis). Letting this angle be denoted ν, it shows:

$$\nu = \tan^{-1}\left(\frac{r\sin v}{r\cos v\cos i}\right) = \tan^{-1}\left(\frac{\tan v}{\cos i}\right) \tag{3.35}$$

The width of the apparent orbit is then the difference between this angle and the mean anomaly M of the reference orbit.

This angle will be maximized near $v = \pi/2$. Since the assumption is the argument of periapsis is $w = \pi/2$, this corresponds to the descending node. Expanding about this point, the small parameter $\varepsilon = v - \pi/2$ is defined, and the angle corresponding to ν as:

$$\tan\varepsilon = \frac{r\sin\varepsilon\cos i}{r\cos\varepsilon} \Rightarrow \varepsilon = \tan^{-1}[\alpha\tan\varepsilon] \tag{3.36}$$

where for brevity use α in place of cos i. This angle is measured from the line of nodes to the projection of the radial vector. The expectation is that $\varepsilon \approx 0$, so that Eq. (3.36) should be valid over the area of interest.

The expansion for ε is:

$$\varepsilon = \alpha\varepsilon + [(\alpha + \alpha^3/3]\varepsilon^3 + O(\varepsilon^5) \tag{3.37}$$

The angular width is found by introducing the expansion for v into this expression. At this point, the assumption is made that the earlier results were "nearly" correct, and thus that δ is in fact of about the same size as e and that $i \approx ce$ for some constant c at least through first order.

Knowing that δ is of the order of e allows the disregard to all terms above third order combined in the two variables. Thus:

$$\begin{aligned}\varepsilon - \delta &= (\alpha - 1)\delta + (1-\alpha^2)\alpha\delta^3/3 + 2\alpha\cos\delta[1 + (1-\alpha^2)\delta^2]e \\ &+ [16(1-\alpha^2)\delta\cos 2\delta - 5\sin 2\delta](\alpha/4)e^2 + [32(1-\alpha^2)\cos^3\delta \\ &- 3\cos\delta - 13\cos 3\delta](\alpha/12)e^3 + \ldots\end{aligned} \tag{3.38}$$

Substituting cos i = cos (ce) for α and expanding the trigonometric terms gives the expansion as:

$$\varepsilon - \delta = 2e - \delta^2 e - (5 + c^2)\delta e^2/2 - (c^2 + 4/3)e^3 \tag{3.39}$$

through third order combined. Through first order, again the width is $2e$, and once more there are no second-order terms.

c. Apparent Vertical Size

The apparent vertical size of the orbit is determined by the elevation angle between the line of sight to the satellite and the reference plane. Relative to the center of the planet, this angle can be expressed as:

$$\kappa_c = \sin^{-1}[\sin u \sin i] \tag{3.40}$$

where u is the angle from the line of nodes to the radial vector. As a result of the requirement on the argument of periapsis, the absolute value will be maximized for $u = \pm \pi/2$. For a circular orbit, it is requires that the maximum value of κ_c equal the maximum value of $v - M$. Thus, from Eq. (3.30):

$$\kappa_c = \sin^{-1}(\sin i) = i = v - M = 2e \tag{3.41}$$

to second order in e.

The vertical angle as seen from the surface of the planet is widened, as is the lateral. However, as the maximum vertical spread occurs at the extrema of the radius, there is a first-order contribution of e to r that must be examined.

When the satellite is at the apses, the apparent elevation angle can be written as:

$$\kappa = \tan^{-1}\left(\frac{R(1+\varepsilon)\sin i}{R(1+\varepsilon)\cos i - R_p}\right) \tag{3.42}$$

where ε is equal in magnitude to the eccentricity, and is positive at apoapsis and negative at periapsis. Expand about $\varepsilon = 0$ to get:

$$\kappa = \tan^{-1}\left(\frac{R\sin i}{R\cos i - R_p}\right) - \frac{RR_p \sin i}{(R-R_p)^2 + R^2 \sin^2 i}\varepsilon + \ldots \tag{3.43}$$

Recalling Eq. (3.41) and making small angle approximations, the first term reduces to:

$$\kappa \approx 2R \cdot e/(R - R_p) \tag{3.44}$$

The second term is the first-order correction to κ.

Note that the coefficient of the correction contains R and R_P. An assumption is made that the product Re / (R - R_P) is small. This is of concern only when R_P approaches R, as for a low-altitude orbit. In this case, it is seen that the correction term is of second order in Re / (R - R_P).

The coefficient of the correction term is negative, showing an expansion of the angle at periapsis and a contraction at apoapsis. The effect of this could be to raise

the apparent orbit slightly with respect to the reference plane. If in fact the apparent orbit is elevated, there should be a corresponding elevation at the points of maximum lateral spread.

To investigate this, a value is required for the position of the satellite on its orbit at which the apparent orbit achieves it maximum width. Return to Eq. (3.38) in an attempt to find this value. If the derivative of this equation is taken, however, no terms are found that are of first order combined. Because the value of ε - δ, and thus of i, is defined only through second order, first-order terms are necessary to obtain any information. Numerical investigations show that the elevation of the point of maximum width is in fact not linear with e [Ref 21].

d. Phase Separation in Apparent Orbit

When there is more than one satellite in apparent orbit about the reference point, they will be separated by some angle, constant to the accuracy of the C–W equations. In Fig. 3.6, the angle denoted ϕ_{12} is such a separation angle.

The separation angle between two satellites in the same apparent orbit is a function of the angle between the lines of nodes of their orbits. Nominally, the separation angle equals this angle. The separation will vary as a result of the second-order deviations of the apparent orbit from perfect circularity; the actual amount of variance will be dependent upon the separation.

Although this makes it impractical to define the change in separation angle, the angular rate of the satellite in its apparent orbit can be considered. The satellite will sweep its angle faster when it is at periapsis than at apoapsis; the ratio will be the same as that for the true anomaly rates:

$$\phi_p/\phi_a = [(1+e)/(1-e)]^2 \tag{3.45}$$

where ϕ is the phase angle in the apparent orbit and the subscripts refer to periapsis and apoapsis.

An estimate of the total variation in $\phi(t)$ from that predicted by the C–W equations can be had by finding the value of the true anomaly when the mean anomaly equals $\pi/2$. This is accomplished through the same expansion used earlier:

$$v = M + 2e\sin M + (5e^2/4)\sin 2M + \ldots \Rightarrow v = \pi/2 + 2e \tag{3.46}$$

through second order. The phase angle in the apparent orbit, measured from the vertical, can be expressed approximately as:

$$\phi(M = \pi/2) = \frac{\pi}{2} + \tan^{-1}\left(\frac{r\sin u \sin i}{R(v-M)}\right) \approx \pi/2 + \sin i \tag{3.47}$$

Recalling that $i \approx 2e$, this implies that the satellite sweeps through $4e$ less apparent angle as M goes from $\pi/2$ to $3\pi/2$ than during the other half of the orbit. Thus, two satellites in orbit about the reference, separated by a 180-degree difference in phase, will vary in their relative positions by $\pm 4e$ radians during the orbit.

e. Geometry of the Orbit

The apparent orbit described in the previous sections is in a sense the projection of the relative orbit onto a plane normal to the radius of the reference orbit (see Fig. 3.3/3.4 above). The actual relative orbit is not circular, but elliptical. This follows from the results gained in Section C above (Linearized Approach).

The depth of the motion is clearly the difference between periapsis and apoapsis, which by definition is 2Re. As the first-order approximation of the diameter of the apparent orbit is 4Re, this implies that the relative motion lies near a plane that is angled 60° with respect to the reference plane. As a result of this, the variation in the actual distance from the reference point to the satellite will vary from a minimum of the apparent orbital radius (when the satellite crosses the reference plane) to a maximum of approximately $\sqrt{5}/2$ times this amount (at periapsis and apoapsis). Thus the actual maximum distance will be (to first order in e) $\sqrt{5}(R - R_p)e$.

4. Example

An example to demonstrate numerically the effects of the correction terms on the linearized solution is presented. To tie all the chapters together, the nanosatellite design's orbital parameters are used in this example.

As has been mentioned in the preceding section, the appearance of the relative orbit is a matter of the angles between the lines of sight to the satellite and to the reference, from a point on the planetary surface along the vector joining the center of the planet to the reference. To speak of the radius of the apparent orbit requires a more precise definition. For this case, simply multiply the angles describing the relative orbit by the altitude of the reference orbit.

Consider a cluster of Earth satellites, such as in Fig. 3.7, in apparent orbit about a central point. The nominal orbital altitude is ~1111 km (600 nm). To exaggerate the second-order effects, set the radius of the apparent orbit at 25 km. Additionally, assume a spherical Earth. The cluster consists of a single ring, with eight satellites equally spaced such that their nominal apparent angular separation is 45 deg.

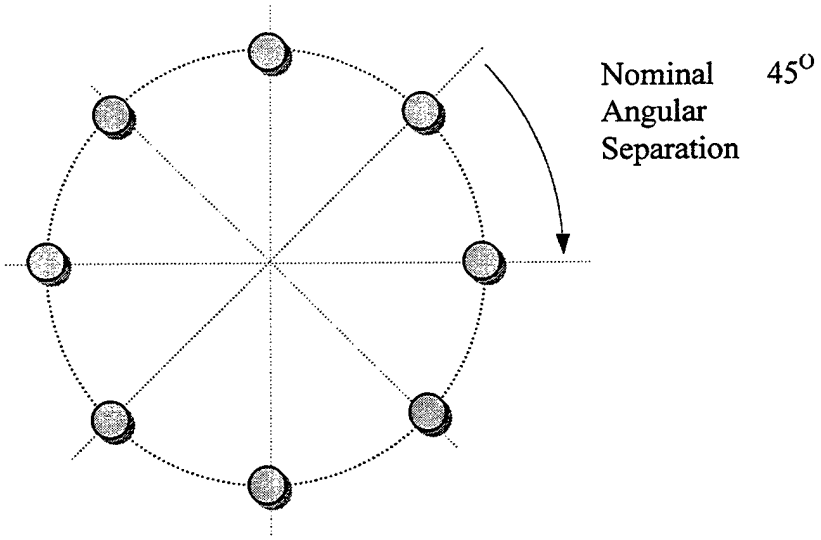

Figure 3.7 Ring of eight equally spaced satellites.

Using the results derived above, have the angular spread of the desired orbit to be λ = 25/1111 = 0.0225023 rad. From Eq. (3.34) the equation works out (with R_p= 6378.1363 km, and R=7489.5457 km) that:

$$0.0225023 = 2\,Re/(R - R_p) \Rightarrow e = 1.67 \times 10^{-3} \text{ rad} = .09563 \text{ deg}$$

The inclination angle is the spread angle, so $i = 2e = 3.34 \times 10^{-3}$ rad = 0.1913 deg. The first-order corrections to the vertical spread of the orbit are:

$$\Delta\kappa = 0.110e = 1.84 \times 10^{-4} = 0.0105 \text{ deg}$$

which when multiplied by the nominal altitude of the orbit produces an apparent shift of 204.07 m. The shape of the apparent orbit is so close to circular that it would appear so to the naked eye.

D. POPULATING AND MAINTAINING A CLUSTER IN LOW EARTH ORBIT (LEO)

The following analysis was used to generate both cartesian and classical orbital elements (Keplerian) that were entered into Satellite Tool Kit® (STK). Both in-plane and out-of-plane clusters were developed and varying plane angles of the remotes were looked at. Creating a Matlab program (see Appendix 3.2) to calculate the data points, some of the final results of the different cluster formations can be found in Appendix 3.3,

For a cluster constellation such as that in Fig 3.8, the initial orbit elements are chosen so that (1) each satellite occupies a node in an arbitrary spatial pattern, and (2) the satellites undergo a cyclic motion that allows the formation to persist with relatively little ΔV for maneuvering. Depending on the application, the center position in the cluster may be occupied by a mother ship or may be empty. An arbitrary distribution of spacecraft in the suborbit plane will maintain its configuration, and the suborbit normal will stay at a fixed angle δ relative to the mothersat orbit normal. Large numbers of physically disconnected nanosatellites can occupy the suborbit plane and can imitate the characteristics of a larger (km-scale) spacecraft.

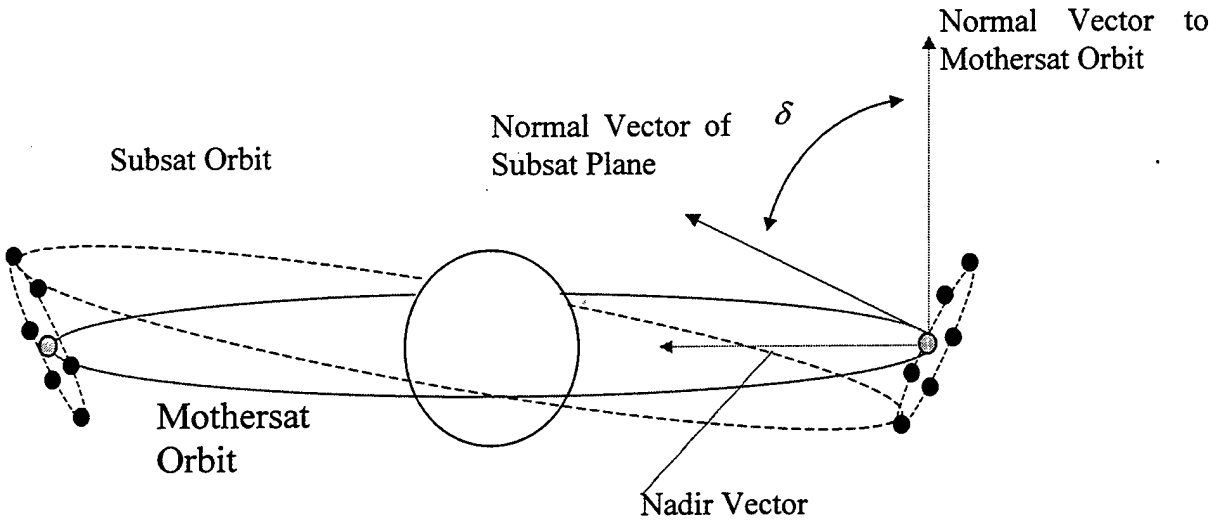

Figure 3.8 Cyclic motion of Subsat Orbit

1. Populating a Remote Cluster

Each subsat (remote) undergoes a cyclic motion in the reference frame of a center satellite (mothersat). The remote completes one suborbit cycle and returns to its original position relative to the mothersat after one revolution about the Earth, as illustrated in Fig. 3.8. Therefore all satellites in the cluster must have the same value for the semimajor axis (and hence the same orbital period) if perturbing forces are neglected. The cluster can be populated based on the idea that each remote is in the 6 o'clock or 12 o'clock position in the suborbit exactly once per revolution. At this instant the remote orbital velocity vector is taken to be parallel to the mothersat velocity vector, but the two velocity magnitudes are different. No further assumptions concerning the position and velocity of the remote at other points in the orbit are needed to determine the orbital elements.

The initial mothersat orbit is specified by the semimajor axis a_c, eccentricity e_c, inclination i_c, right ascension of the ascending node Ω_c, argument of perigee w_c, and mean anomaly at epoch M_{c0}. Three parameters that specify the cluster geometry (ρ, η, δ)

are illustrated in Fig 3.9. The scale factor ρ determines the overall cluster size of and is assigned the same distance value for all remotes (i.e. 25 km), while the dimensionless pattern generator η can be different for each remote and determines the geometrical arrangement (i.e. for circular rings, η=1). The angle δ specifies the shape of the suborbit and the orientation of the suborbit plane relative to the orbit plane of the mothersat. Choosing different values for δ in one cluster will produce a swarm having multiple suborbit planes.

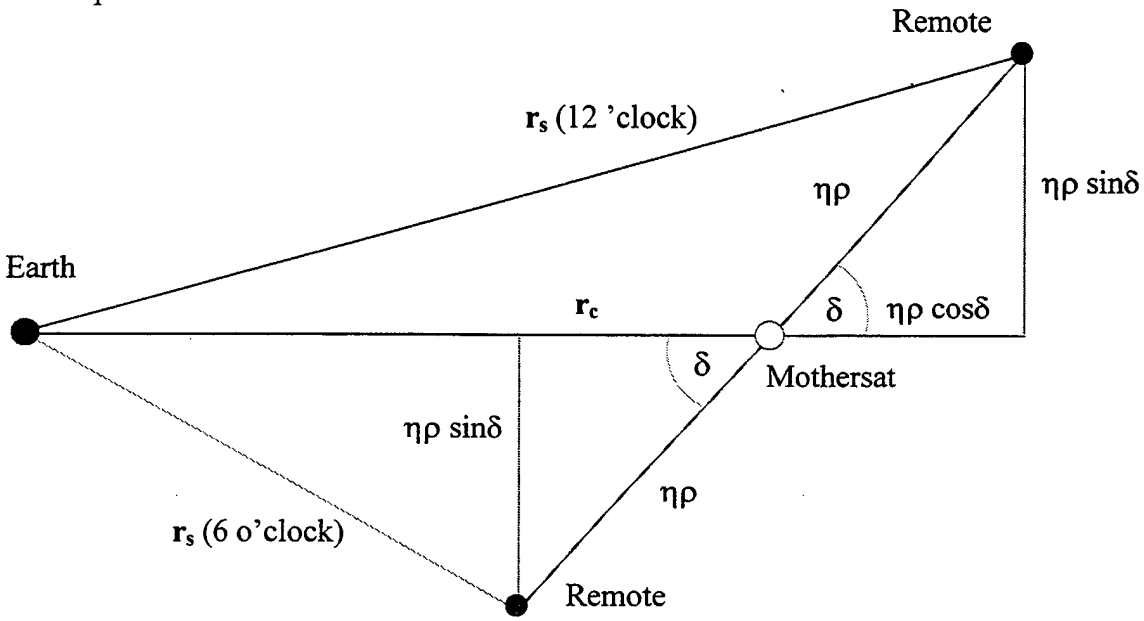

Figure 3.9 Remote Geometry as viewed along Mothersat Velocity vector

The following paragraphs utilize definitions and equations from Vallado's Astrodynamics textbook. [Ref. 21] Determining the remote orbital elements begins by choosing a set of E_c values (e.g. 0°, 45°, 90°, etc.) where E_c is the eccentric anomaly of the mothersat at the location in the orbit when the corresponding remote is at the 6 or 12 o'clock position (either may be used to populate the cluster). At these 'population points' the true anomaly, mean anomaly, radius and orbital speed of the mothersat are:

$$\theta_c = 2\tan^{-1}\left[\frac{1+e_c}{1-e_c}\tan\left(\frac{E_c}{2}\right)\right] \tag{3.48}$$

$$M_c = E_c - e_c \sin E_c \tag{3.49}$$

$$r_c = \frac{p_c}{1 + e_c \cos\theta_c} \tag{3.50}$$

$$v_c = \sqrt{\mu\left(\frac{2}{r_c} - \frac{1}{a_c}\right)} \tag{3.51}$$

where $p_c = a_c(1 - e_c^2)$. From Fig 3.9 the radius and orbital speed of the remote at the population point are:

$$r_s = \sqrt{(\eta\rho\sin\delta)^2 + (r_c \pm \eta\rho\cos\delta)^2} \tag{3.52}$$

$$v_s = \sqrt{\mu\left(\frac{2}{r_s} - \frac{1}{a_s}\right)} \tag{3.53}$$

where the ± sign in Eq (3.52) is negative for the 6 o'clock and positive at 12 o'clock. Here it is assumed that $a_s = a_c$ for all remotes, but this choice will be modified later. Using the above expressions together with the construction in Fig. 3.9, the radius and velocity vectors in the mothersat perifocal coordinates when a remote is at the population point are:

$$\vec{r}_c = r_c \begin{bmatrix} \cos\theta_c \\ \sin\theta_c \\ 0 \end{bmatrix}$$

$$\vec{v}_c = \sqrt{\frac{\mu}{p_c}} \begin{bmatrix} -\sin\theta_c \\ e_c + \cos\theta_c \\ 0 \end{bmatrix} \tag{3.54}$$

$$\vec{r}_s = \begin{bmatrix} (r_c \pm \eta\rho\cos\delta)\cos\theta_c \\ (r_c \pm \eta\rho\cos\delta)\sin\theta_c \\ \pm\eta\rho\sin\delta \end{bmatrix}$$

$$\vec{v}_s = \frac{v_s}{v_c}\vec{v}_c \tag{3.55}$$

The magnitudes of these vectors agree with the scalar values in Eqns. (3.50)-(3.53). Equation (3.55) expresses the key idea that the remote and mothersat velocity vectors are parallel at the population points.

Knowing that the radius vector and velocity vector of a remote at one point in its orbit is sufficient for calculating its orbital elements (a_s, e_s, i_s, Ω_s, w_s, M_{s0}). The first step is to transform the remote radius and velocity vectors from mothersat perifocal coordinates to Earth-centered inertial coordinates as follows:

$$\vec{r}_{ijk} = \vec{R} \cdot \vec{r}_s$$
$$\vec{v}_{ijk} = \vec{R} \cdot \vec{v}_s \tag{3.56}$$

where $\vec{R}$ is a 3x3 rotation matrix[1] defined by:

$$\vec{R} = R(\Omega_c) * R(i_c) * R(w_c) \tag{3.57}$$

and with the three components identified as:

$$R(\Omega_c) = \begin{bmatrix} \cos(-\Omega_c) & \sin(-\Omega_c) & 0 \\ -\sin(-\Omega_c) & \cos(-\Omega_c) & 0 \\ 0 & 0 & 0 \end{bmatrix}$$

$$R(i_c) = \begin{bmatrix} 1 & 0 & 0 \\ 0 & \cos(-i_c) & \sin(-i_c) \\ 0 & -\sin(-i_c) & \cos(-i_c) \end{bmatrix} \tag{3.58}$$

$$R(w_c) = \begin{bmatrix} \cos(-w_c) & \sin(-w_c) & 0 \\ -\sin(-w_c) & \cos(-w_c) & 0 \\ 0 & 0 & 1 \end{bmatrix}$$

The second step is to apply the set of equations relating the Earth-centered inertial radius and velocity vectors to the classical orbital elements. This procedure yields (a_s, e_s,

[1] Matrix found in Matlab program in Appendix 3.2

i_s, Ω_s, w_s, θ_s) where θ_s is the true anomaly at the population point. The corresponding eccentric anomaly and mean anomaly are:

$$E_s = 2\tan^{-1}\left[\sqrt{\frac{1-e_s}{1+e_s}}\tan\left(\frac{\theta_s}{2}\right)\right] \tag{3.59}$$

$$M_s = E_s - e_s \sin E_s \tag{3.60}$$

The cluster is initialized with the mothersat at perigee, and hence the initial mothersat mean anomaly is M_{c0}=0°. Using Eq. (3.49) for M_c at the population point and Eq. (3.51)for M_s at the same point, the initial remote mean anomaly is $M_{s0} = M_s - M_c$, which completes the determination of the remote orbital elements. The resulting e_s, i_s, Ω_s, w_s, M_{s0} are distributed around the mothersat values, with the difference depending on the magnitude of ρ and on the location on the remote within the cluster.

The initial subsat orbital elements can be refined to enhance cluster stability in the presence of the non-spherical geopotential. This is accomplished by calculating the subsat displacements (relative to their original positions) after one orbital period of the mothersat. The most significant perturbation (which will be discussed in a later section) is due to the second zonal harmonic J_2, which appears in the expressions for the mean mean-motion $\bar{w}$ and the secular rates of change of Ω and w.

Propagating the cluster for one revolution in low-Earth orbit under the influence of J_2 reveals that the remote displacements are primarily in the mothersat along-track coordinate (y-axis), with cross-track and radial displacements being at least 50 times smaller. This suggests that the semimajor axis of each remote can be adjusted slightly to cancel the along-track displacement. In the unperturbed solution the semimajor axis was the same for all satellites in the cluster, namely $a_s = a_c$ in Eq. (3.53). The revised semimajor axis that compensates for along-track displacements due to J_2 is:

$$a_s = a_c + \frac{\Delta Y}{3\pi} \tag{3.61}$$

where ΔY is the along-track displacement after one revolution. Typically the revised semimajor axis differs from a_c by less than 5m at 1111 km altitude. Of course, adjusting a_s does not reduce the cross-track and radial displacements caused by J_2.

E. PERTURBATIONS AND ΔV REQUIREMENTS

1. STK Perturbation Propagators

For real analysis the non-spherical geopotential and other perturbing forces conspire to disrupt cluster coherency. Data from STK's numerous perturbation modelers propagated the orbits and presented influences based on two-body, J_2 and J_4 contributions, solar/lunar gravitational effects, solar radiation pressure, and atmospheric drag for short term (3-10 days) and long term (1 year) investigation.

a. Two-Body, J_2 and J_4

A Two-Body, or Keplerian motion, propagator considers only the force of gravity from the Earth, which is modeled as a point mass. The two-body propagator uses the same basic technique outlined in the two-body equation of motion development. This technique assumes the Earth is a perfect sphere and the only force acting on a satellite is gravity. This propagator doesn't account for any perturbations.

J_2 Perturbation (first-order) and J_4 Perturbation (second-order) propagators account for secular (long-term) variations in the orbit elements due to Earth oblateness. These propagators don't model atmospheric drag or solar or lunar gravitational forces.

J_2 and J_4 are zonal harmonic coefficients in an infinite series representation of the Earth's gravity field. J_2 represents the dominant effects of Earth oblateness. The even zonal harmonic coefficients of the gravity field are the only coefficients that result in secular changes in satellite orbital elements. The J_2 propagator includes the first-order secular effects of the J_2 coefficient while the J_4 propagator includes the first- and second-order effects of J_2 and the first-order effects of J_4. The J_3 coefficient, which produces long period periodic effects, isn't included in either

propagator. J_4 is approximately 1000 times smaller than J_2 and is a result of Earth oblateness. Since the second-order J_2 and the first-order J_4 secular effects are very small, there is little difference between the orbits generated by the two propagators.

b. HPOP

HPOP is the High Precision Orbit Propagator, and was the main propagator for formation analysis for this thesis. HPOP, included as part of STK/PRO, can handle circular, elliptical, parabolic and hyperbolic orbits at distances ranging from the surface of the Earth to the orbit of the Moon and beyond. As its name implies, it uses a powerful propagation technique to incorporate sophisticated orbit perturbation models. HPOP uses a Runge-Kutta-Fehlberg integration method of order 7-8 to propagate the satellite state in the J2000 reference frame. A variety of high-fidelity models are utilized, including the Joint Gravity Model 2 (JGM2; a highly precise model (70 x 70) of the Earth's oblateness) with a maximum degree/order of 21.

The atmospheric density model used the Jacchia-Roberts (similar to Jacchia-1971 but uses analytical methods to improve performance) to model drag effects on the spacecraft. This model takes into account daily variations in the height of the atmosphere due to solar heating among other parameters, and was based on values of $C_d = 2.0$, daily/average F10.7 of 150, a geomagnetic index of 3.0 and an area/mass ratio of 0.020 m^2/kg.

Solar radiation pressure was modeled using $C_r = 1.0$ and the same area/mass ratio as above. Since sunlight produces a small force on any exposed surface. This force varies depending on how reflective the surface is (i.e. a mirrored surface is more reflective than a black surface). The solar radiation pressure model in HPOP has been updated to be consistent with other commonly used propagators such as GTDS.

Finally, third body gravity models (solar/lunar gravitational effects) are based on U.S. Naval Observatory data and are accurate to within 0.03 arc seconds. Additionally, third-body gravitational perturbations are also computed using the DE 405 planetary ephemeris from JPL for the Sun and Moon.

2. Perturbation Effects

Propagations in the presence of perturbations show the circular formation to be highly unstable. The primary factor disrupting the formation design is the earth's oblateness or J_2 effect. The J_2 contributions to the relative motion are at least an order of magnitude larger than the disturbing accelerations including tesseral resonance (for short repeat ground track cases), atmospheric drag, solar radiation pressure, and third body gravitational effects. Earth oblateness effects are most prevalent in the secular motion of the right ascension of the ascending node (Ω), argument of perigee (w), and mean anomaly (M).

The cross-track error growth can be attributed to the difference in precession rates of the right ascension of the ascending node. Since the two orbital planes have slightly different inclinations, the secular J_2 effect causes the right ascension of the ascending node for each orbit to precess at slightly different rates. This results in the orbital planes drifting apart and a cross-track error growth.

An additional contribution to the error growth is caused by the rotation of the line of apsides of the orbits. This is close to causing the J_2 effect to be equal but opposite on the mean anomaly and the argument of perigee. If the orbit is not circular (i.e. all the remotes' orbit) the orbit line of the apsides begins to rotate and disrupt the formation design.

Large variations in eccentricity and argument of perigee that occur in near-circular LEO will disrupt the formation, but they can be greatly reduced by placing the mothersat into a 'frozen' orbit. This choice also simplifies the ephemeris representation, because here are no secular or long-period variations in e_c and ω_c. The NASA/JPL TOPEX mission has successfully demonstrated the long-term stability and maintenance of this type of orbit. [Ref. 22] A frozen orbit requires $w_c = 90^\circ$ and a particular value of e_c that is determined by the choice of inclination and altitude. Although only one of the satellites in the cluster (typically the mothersat) can achieve frozen conditions, it is expected that the total ΔV of formation keeping will be minimized for this choice.

Periodic maneuvers must be performed by the mothersat to follow a reference orbit having an altitude and frozen eccentricity. Typical the mothersat will have a higher area-to-mass ratio then the remotes, and its altitude will therefore decay more quickly. Drag compensation is applied so that the mothersat reference orbit matches the average decay rate of all the remotes. This minimizes the fuel requirements for each remote.

For the long-term behavior (~3 years), solar radiation pressure and atmospheric drag will disturb the frozen orbit conditions, because the eccentricity and argument of perigee are no longer constant. Small oscillations in inclination are common to the mothersat and remotes and are not expected to disrupt the formation.

For the short-term behavior (1-10 days), effects of atmospheric drag, solar radiation pressure, and the J_2 to J_6 gravitational harmonics disrupt the cluster geometry. The position deviations indicate that frequent formation-keeping maneuvers are needed to maintain the desired separations among the remotes. Drag is the largest contributor to the position deviations at 1111 km altitude, and this is compensated efficiently using mothersat maneuvers. The cross-track deviation is caused primarily by differential nodal regression:

$$t_m = 4\sqrt{\frac{2L}{3q\omega}} \tag{3.62}$$

$$\Delta V_m = \frac{q\omega t_m}{2} \tag{3.63}$$

where t_m is the time between maneuvers, L is the in-track tolerance in meters, q is the orbit decay rate in m/sec, ω is the orbit mean motion in rad/sec, and ΔV_m is the velocity increment of each two-burn transfer. The total ΔV for the remotes are obtained by summing the velocity increments for each maneuver.

3. Formation Keeping

The circular and projected circular formations were highly unstable and require formation-keeping maneuvers to account for earth oblateness, atmospheric drag, and tesseral resonance (for short repeat ground track cycle orbits) effects.

Both atmospheric drag and tesseral resonance affect the formation in the along-track direction. The along-track error growth induced by these perturbations can be controlled via small adjustments in the semimajor axis of the satellites. Based on the results of the propagation, these semimajor axis adjustments are sub-centimeter for drag effects and on the centimeter level for deep tesseral resonance. From Gauss' variation of parameters (VOP) equations [Ref 23] for Keplerian elements in the normal-tangential plane, the change in semimajor axis due to a disturbing acceleration is:

$$\frac{da}{dt} = \frac{2a^2V}{\mu} a_{dt} \tag{3.64}$$

where a is the semimajor axis, V is the magnitude of the velocity, μ is the gravitational constant for the earth, and a_{dt} is the acceleration in the direction of the velocity vector.

If a velocity impulse is assumed, Eq. (3.64) can be rearranged to determine the velocity impulse required to produce a desired change in semimajor axis:

$$\Delta V_t = \frac{\mu}{2a^2V} \Delta a \tag{3.65}$$

where the changes in velocity, ΔV, and semimajor axis, Δa, are assumed small compared to the nominal values. From Eq. (3.65), it can be shown that to change the semimajor axis by 10cm, a velocity impulse of 0.00478 cm/sec is required for an 1111 km altitude near-circular orbit. Thus, the ΔV, and therefore propellant requirements, to account for the differential drag and tesseral resonance effects will be quite small. The frequency of the maneuvers will depend on the extent of the drag and resonance effects, formation keeping error bounds, and several control related issues, such as the accuracy with which these maneuvers are affected.

The effects of J_2 were seen in the cross-track direction with indirect along-track contributions. In terms of Keplerian elements, the J_2 secular effects on right ascension of the ascending node, argument of perigee, and mean anomaly are of concern. From Battin [Ref. 23], the change in right ascension of the ascending node due to an out of plane (cross-track) acceleration is:

$$\frac{d\Omega}{dt} = \frac{r\sin(w+v)}{h\sin(i)} a_{dh} \tag{3.66}$$

where r is the satellite radius magnitude, w is the argument of perigee, v is the true anomaly, h is the angular momentum, i is the orbit inclination, and a_{dh} is the acceleration in the direction of the angular momentum vector. If a velocity impulse is assumed, Eq. (3.66) can be rearranged to determine the velocity impulse required to produce a desired change in right ascension of the ascending node:

$$\Delta V_h = \frac{h\sin(i)}{r\sin(w+v)} \Delta\Omega \tag{3.67}$$

where the changes are assumed small. The differential oblateness effects on right ascension of the ascending node can be derived analytically by taking the partial derivative of the governing equation with respect to the inclination (taken from Vallado [Ref. 21]):

$$\begin{aligned} \dot{\Omega} &= -\frac{3}{2} J_2 \left(\frac{R_e}{p}\right)^2 w\cos(i) \\ \partial\dot{\Omega} &= \frac{\partial\dot{\Omega}}{\partial t}\partial i = \frac{3}{2} J_2 \left(\frac{R_e}{p}\right)^2 w\sin(i)\partial i \end{aligned} \tag{3.68}$$

Combining Eqs. (3.67)-(3.68), it is seen that the amount of velocity impulse required to maintain nodal spacing is proportional to the size of the formation and the length of the mission:

$$\begin{aligned} \Delta\Omega &= \partial\dot{\Omega}\Delta t \\ \Delta V_h &= \frac{h\sin(i)}{r\sin(w+v)} \frac{3}{2} J_2 \left(\frac{R_e}{p}\right)^2 w\sin(i)\partial i\Delta t \end{aligned} \tag{3.69}$$

where δi is the inclination difference in the formation and Δt is the time between maneuvers. If the near circular assumption is made, Eq. (3.69) simplifies to:

$$\Delta V_h = \frac{w^2\sin^2(i)}{a\sin(w+v)} \frac{3}{2} J_2 \cdot R_e^{\,2} \cdot \partial i \cdot \Delta t \tag{3.70}$$

The total ΔV requirement is approximately ~7.2m/sec per kilometer of separation per year for an 1111-kilometer altitude circular formation. It should be noted that the maneuvers must be performed at certain points in the orbit to avoid disturbing the inclination.

The second disruptive influence of the earth's oblateness on satellite formation flying is the rotation of the orbit line of apsides. Since the effects of J_2 on the argument of perigee and mean anomaly are nearly equal and opposite:

$$\begin{aligned} \dot{w} &= \frac{3}{4} J_2 \left(\frac{R_e}{p} \right)^2 \omega \left(4 - 5\sin(i) \right) \\ \dot{M}_0 &= \frac{3}{4} J_2 \left(\frac{R_e}{p} \right)^2 \sqrt{1-e^2}\, \omega \left(3\sin^2(i) - 2 \right) \end{aligned} \tag{3.71}$$

The effects of accelerations in the normal direction are also nearly equal and opposite on these elements for near circular orbits:

$$\begin{aligned} \frac{dw}{dt} &= \frac{1}{eV} \left(2e + \frac{r}{a}\cos(v) \right) a_{dn} \\ \frac{dM}{dt} &= \frac{-b}{eaV} \left(\frac{r}{a}\cos(v) \right) a_{dn} \end{aligned} \tag{3.72}$$

In Eq. (3.72), only accelerations in the normal direction (mutually perpendicular to $\bar{h}$ and $\bar{v}$ are considered since impulses in the tangential (velocity) direction would affect semimajor axis maneuvers in the cross track direction do not affect the mean anomaly.

Since the effects of these maneuvers are nearly equal and opposite on the mean anomaly and argument of perigee, the formation keeping analysis can be focused on maintaining either one of the elements with maneuvers in the normal direction. This assumes that the other element will be maintained by those maneuvers as well. For now, the argument of perigee is looked at.

If impulse maneuvers are assumed, Eq (3.72) can be rewritten in terms of the amount of velocity impulse required for a given change in argument of perigee:

$$\Delta V_n = \frac{eV}{\cos(v)} \Delta w \tag{3.73}$$

where the eccentricity is considered to be small. The required change in argument of perigee can be derived from Eq. (3.71):

$$\Delta w = \dot{w}\Delta t = -\frac{3}{4}J_2\left(\frac{R_e}{p}\right)^2 \omega\Delta t$$
$$\Delta V_n = -\frac{eV}{\cos(v)}\frac{3}{4}J_2\left(\frac{R_e}{p}\right)^2 \omega\Delta t \tag{3.74}$$

where the amount of ΔV required is again a function of the length of the mission. For an 1111 km altitude circular mission, the total Δv requirement is approximately 2.1m/sec per year. It should be noted again that the maneuvers must be performed at certain points in the orbit to avoid disturbing the eccentricity.

4. Station Keeping

The primary station keeping concerns for all formation flying designs is atmospheric drag. For an 1111 km altitude satellite, atmospheric drag could decay the orbit's semimajor axis by close to 0.2 kilometers in one year. Of course the effects of drag are dependent on the satellite altitude, area to mass, drag coefficient, and the atmospheric density, which is a function of the solar cycle. A high-density atmosphere near the peak of the solar cycle was used in this analysis so the drag estimates may be overly conservative. Station keeping a 0.2 km/year decay in semimajor axis could require approximately .097 m/sec of velocity impulse.

F. OTHER TOPICS

Another topic specifically important to formation problems is reconfiguration. Formations are designed based on the optimization of the various performance metric functions for a given mission. These performance metric functions are defined to meet the mission requirements. Various primary mission requirements, such as achieving the best image quality or gaining the highest probability of detecting moving targets, lead to different performance metric functions. As a result, image or interferometry qualities for

example, is closely related to the formation baseline and the distribution of the satellites in the formation, whereas the performance of moving target indication systems depends on the number of satellites and the footprint. To meet multiple mission requirements, it is important for the formation controller to have the capability of easy reconfiguration. Furthermore, if one satellite has a malfunction in the middle of a mission, the adjustment of the satellite distribution to keep the system working, or the replacement of the satellite with the malfunction, requires reconfiguration of the formation. Reconfiguration could include adjustment of the relative distance between satellites, reassignment of the leader of a formation, the changing of the numbers of satellites in the formation, and the combination of two formations flying closely.

IV. SUBSYSTEM DESIGN

To incorporate a useable and attainable design for potential nanosatellite clusters, two satellite subsystems show up as integral to the proposal: 1) the attitude determination and control subsystem, and 2) the propulsion subsystem. Although all subsystems of a satellite bus are mutually coupled with all other subsystems onboard, these two systems allow the close formation flying needed for the numerous cluster missions so far mentioned.

The assumptions offered in the remaining chapter's component selection are derived from given reference payload requirements, the constraint of the previous chapter's calculations of ΔV required over a course of a year to maintain the cluster formation, and to minimize mass, power and physical size. Table 4.1 sums up most physical assumptions of the overall spacecraft.

Characteristic	**Value**
Satellite shape and composition	Cylindrical and homogenous
Mass	10 kg
Radius	0.21 m
I_{XX}, I_{YY}	0.16 kg m^2
I_{ZZ}	0.22 kg m^2
Height	0.25 m
Moment arm (z-axis)	0.208 m
Moment arm (x,y-axis)	0.104 m
Propulsion & ADCS Mass Allowance	35% (3.5kg)

Table 4.1 Assumptions made for Satellite Physical Characteristics

A. ADCS

The requirements of ADCS systems are twofold:

Support formation flight

- Manage attitude/rates to the extent required to support precision propulsive maneuvers if available/ required.
- Maintain pointing within small angles (i.e. $\pm .5^{\circ}$ in pitch and roll, $\pm 1^{\circ}$ in yaw), and maintain rates to within precise control (i.e. $\pm 0.1^{\circ}$ per second) of the desired rates about each axis.
- Maintain attitude knowledge and spacecraft stability at all times

Support ground communication

- Point communication antenna for command uplink and telemetry downlink when within sight of ground station

Attitude Control is required for any satellite system and small satellites are no exception. Until now most small (i.e. micro-/nanosats) used only very simple and rudimentary attitude control systems. This can now change with the development of Microelectromechanical Systems (MEMS) and other small consumer electronics devices and manufacturing techniques. New control systems are now needed for missions such as nanosatellite formation flying missions and space-based interferometry.

Nanosatellites represents a flexible tool to carry out scientific and technological research in space. Nevertheless, obvious limitations in size, mass, onboard available power, and costs impose several constraints on the design of nanosatellite subsystems. The attitude control subsystem, as one of the more complex subsystems of a satellite, is particularly affected by these constraints, especially when the considered applications require stringent attitude control. Therefore new solutions in terms of components and operating logic need to be investigated to reduce costs, volume, and power requirements.

The Attitude Determination and Control Subsystem measures and controls the spacecraft's angular orientation (pointing direction), or, in the case of guidance, navigation, and control system, both its orientation and linear velocity (which affects its orbit). The simplest spacecraft are either uncontrolled or achieve control by passive methods as spinning or interacting with the Earth's magnetic or gravity fields. These may or may not use sensors to measure the attitude or position. More complex systems employ controllers to process the spacecraft attitude, and actuators, torquers, or propulsion subsystem thrusters to change attitude, velocity or angular momentum.

1. Magnetic Control

Because of its low mass and power consumption requirements, magnetic control is of particular interest for small satellites, since it is extensively adopted also for active attitude damping in gravity gradient stabilized satellites, initial despin, attitude acquisition, and procession control. [Ref. 24/25] Several authors have studied and documented the attitude control of microsatellites, and a case for nanosatellites can then be made from those results. The use of environmental torques, such as those caused by gravity, the Earth's magnetic field, and aerodynamic drag, to control the spacecraft attitude by means of passive and/or semi-passive devices allows substantial mass and power savings. With regard to this, various solutions have been proposed based on the use of gravity gradient booms with eddy current dampers, fluid ring dampers, or soft-magnetic damping rods to damp the satellite residual attitude motion. Nevertheless, these solutions achieve poor attitude control accuracy (~ 5-10deg). When a finer control is required, as in the case of remote sensing applications (~ 0.1 deg), various configurations of low-mass, low-power momentum/reaction wheels have been proposed. In this case the use of magnetic torquers for momentum dumping, as an alternative to more traditional gas jets [Ref. 26], reduces the control system complexity and mass. Components available for use in these situations will be presented later on this section (Section A3 below).

a. All-Magnetic Torquer System

To develop 3-axis attitude control given the very limited power and weight availability on a nanosatellite, an all-magnetic torquer system where permanent magnets on stepper motors could be used instead of traditional torquer coils. The attitude determination would be achieved by a combination of Earth horizon and sun sensors, giving three-axis control to approximately two to three degrees. Although this concept does not provide fine control ability for most remote sensing applications, the idea is to progress the knowledge base by getting these nanosatellite systems into space and start operational testing and evaluation.

b. Reaction wheel / Magnetic Torquerod System

As a last example, the attitude control system of the Italian Scientific Microsatellite for Advanced Research and Technology (SMART) was reviewed. Their microsatellite attitude control system consisted of three small reaction wheels and three magnetic torquers (torquerods). The wheels were used for three-axes attitude control during station keeping. The reaction wheel design had been performed using a technique that minimized mass and power consumption. As far as the magnetic torquer design was concerned, it was primarily driven by the requirements for onboard wheel momentum unloading and initial attitude acquisition following the separation from the launcher. Nevertheless, the possibility of using the magnetic torquers for attitude control during station keeping was considered. Their technique was to distribute the torque required for attitude control between wheels and magnetic torquers, which minimized the total power consumption. The result of this example [Ref. 27] presented the analytical model of the proposed technique and demonstrated its effectiveness by numerical simulations. In particular, the numerical analysis shows the following:

- Wheels and torquerods can be simultaneously used to realize a required control torque with minimum power consumption.
- The control torque distribution between torquerods and wheels is governed by the torquerod control efficiency, which strongly depends on the Earth's magnetic

field variation along the orbit and on the torquerod design parameter R_t / scf^2 (where R_t is the torquerod winding resistance and *scf* is the ratio of the torquerod magnetic dipole to the torquerod supply current).

- When more efficient torquerods are used, the control torque portion transferred to the torquerods increases so that the total power consumption is minimized.
- The use of torquerods with low values of the design parameter allows substantial power savings with respect to the case of optimal control with reaction wheels only.
- As the required torque percentage assigned to the torquerods increases, the attitude control accuracy reduces. Nevertheless, substantial power savings can be realized while retaining attitude control accuracy adequate for remote sensing applications (0.016 deg for a 40% power savings).
- The attitude control accuracy could be improved by slightly increasing the numerical values of the control gains at the cost of higher power consumption.
- The proposed control technique could be used in addition to wheel momentum unloading and attitude acquisition considerations to design the satellite torquerods

Finally, the proposed technique does not increase the attitude control system complexity and mass because the torquerods are also used for initial attitude acquisition and wheel momentum unloading.

2. Propulsion Option

The attitude control system is very closely coupled with several of the other systems aboard the spacecraft, and influences or is influenced by every system on the spacecraft to some degree. In the remote's attitude control configuration, the most notable interaction is normally that with the Propulsion system. One concept that many nanosatellite designers are utilizing consists of micro-pulsed-plasma thrusters (μPPTs) to provide control of both attitude and translation. The shared nature of the ADCS and propulsion actuators also has a profound effect on the formation flight mission, placing

limits on the controller design. This design option is explained more in detail under the Propulsion section below (Section B1 below).

3. Components

Appendix 4.1 shows the overview of ADCS components covered in this section.

a. Micromechanical gyroscope

Micromachined solid-state gyroscopes use vibrating mechanical elements to sense rotation. They have no rotating parts that require bearings, so they can be easily miniaturized. All vibration gyroscopes are based on the transfer of energy between two vibration modes of a mechanical structure, caused by Coriolis acceleration [Ref. 28]. The highest rotation sensitivity is obtained when the drive and sense modes have the same resonant frequency.

Resolution, drift rate, zero-rate output, and scale factor are the most important factors that determine the performance of a gyroscope. When a gyroscope is inertially static, the output signal is a random function that is the sum of white noise and a cyclic noise function of the mechanical resonant frequencies.

Based on resolution, drift rate, and zero-rate output, the Systron Donner QRS-11 micromachined angular rate sensor (see Fig. 4.1) was seen as the leader from seven commercially available micromachined gyroscopes to complement magnetometers for yaw determination. This gyroscope has a resolution of 0.004°/s, a short-term bias stability (100s at constant temperature) of 0.004°/s, and a zero-rate output (DC to 100 Hz) of 0.01°/s. The gyroscope has a mass of 60g [Ref 29].

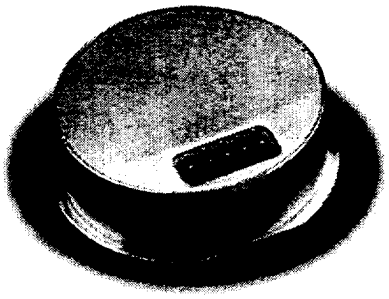

Figure 4.1 BEI GYROCHIP™ Model QRS11 Micromachined Angular Rate Sensor

A close alternative to the QRS-11, would be the Litton G2000 gyro (see Fig. 4.2). This component offers a two-axis gyro with a size of only 0.97 inches tall by 0.76 inches wide and weighs 25 grams [Ref. 30]. This gyro system can be combined with a star sensor system to provide attitude position information to provide a pointing accuracy of approximately 0.1 degree. The system is still in production and testing and has not been space flown.

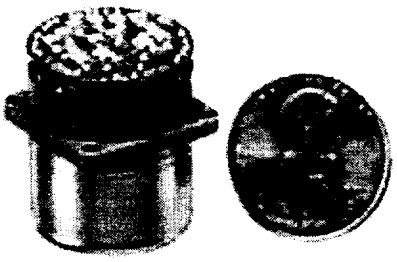

Figure 4.2 Litton G2000 gyroscope with electronics

b. Magnetometers

Magnetometers are simple, lightweight sensors that measure both the direction and magnitude of the Earth's magnetic field. They are reliable but require complex software for interpretation and provide relatively coarse attitude determination as compared to horizon, sun, and star sensors. GPS position measurements are used with a computer model of the Earth's magnetic field to approximate the field direction at the spacecraft's current position. Over the course of an orbit, the Earth's magnetic field

direction usually changes rapidly enough with respect to the spacecraft to make computation of the field's time derivative possible. These field variations are large enough to enable determination of all three Euler angles using only a three-axis magnetometer. The Earth's magnetic field also varies with time and cannot be calculated precisely, so a magnetometer is often used with another sensor such as a sun, horizon or star sensor or a gyroscope in order to improve the accuracy.

The Applied Physics Systems Model 533 miniature three-axis fluxgate magnetometer (see Fig. 4.3) can provide direction accuracy to better than 0.1° in a laboratory environment. This model is well suited for use in the nanosatellite because of its extremely low mass (18g) and its small size [Ref. 31]. Yaw attitude knowledge is maintained between magnetometer readings by integration of angular rate measurements.

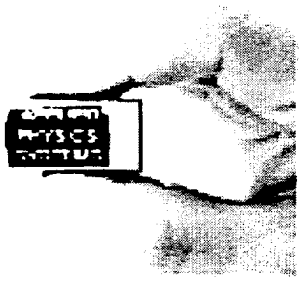

Figure 4.3 Model 533: Miniature 3 Axis, Fluxgate Magnetometer

c. Reaction Wheels

The reaction wheel is used as an actuator for the attitude control and is one of many important key technologies of nanosatellites. Hokkaido Institute of Technology (HIT) has developed a small reaction wheel, which is about 150g in weight and 0.015 Nms in maximum storable angular momentum. The motor, which can be used in a vacuum, is 30g and has a torque of 28gcm/2W. The wheel mass balance is adjusted precisely and the vibrational level is restricted as low as possible.

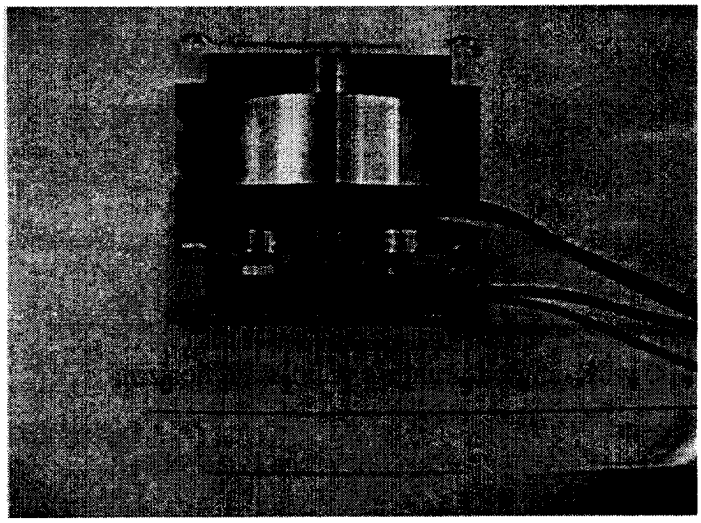

Figure 4.4 Small reaction wheel developed by HIT

d. Sensors

(1) Horizon sensors

Horizon sensors are infrared devices that detect the contrast between the cold of deep space and the heat of the Earth's atmosphere. Horizon sensors can provide pitch and roll attitude knowledge for Earth-pointing spacecraft, with an accuracy of 0.1° to 0.25°. For the highest accuracy in low Earth orbit (LEO), it is necessary to correct the data for the Earth oblateness and seasonal changes in the apparent horizon.

Two EDO Barnes Model 13-500 wide-angle miniature solid-state horizon sensors (see Fig. 4.5) can be used to provide pitch and roll knowledge to ± 1°, including all errors. These sensors have been space-proven on six missions to date. The sensors have fields of view sufficient to allow pointing at off-nadir angles of up to ± 11°, but peak performance is limited to angles less than 9°. Each sensor has a mass of 0.113 kg and is roughly cylindrical with a diameter of about 4.1 cm and a height of about 5.6 cm [Ref. 32].

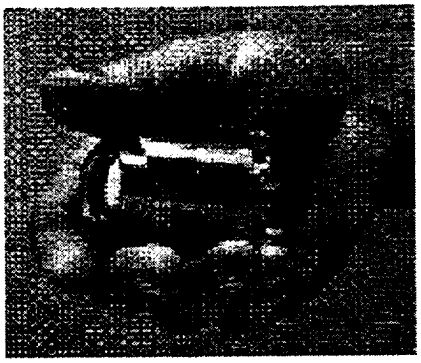

Figure 4.5 EDO Barnes Model 13-500 wide-angle miniature solid-state horizon sensor

(2) Star Tracker

Current state-of-the-art commercial star sensors typically weigh 15 pounds, attain 5 to10 arc-second accuracy, and use roughly 10 watts of power. Unfortunately, the current state-of-the-art commercial star sensors do not meet many of NASA's "next-generation" spacecraft and instrument needs. Nor do they satisfy DoD's need for micro/nano-satellite systems. The *Intelligent Star Tracker* [Ref. 33], built by AFRL, presents a low cost, miniature star tracker for nanosatellite attitude determination and navigation. The *Intelligent Star Tracker* incorporates adaptive optic catadioptric telescopes in a single, compact, robust Silicon Carbide housing. The Micro-opto-electro-mechanical (MOEMs) micro-mirrors (see Fig. 4.6) are used to compensate for various aberrations as well as introduce aberrations such as leveraging off of adaptive optics research, the active pixel position sensors enable wide dynamic range and simultaneous imaging of faint and bright stars in a single image frame.

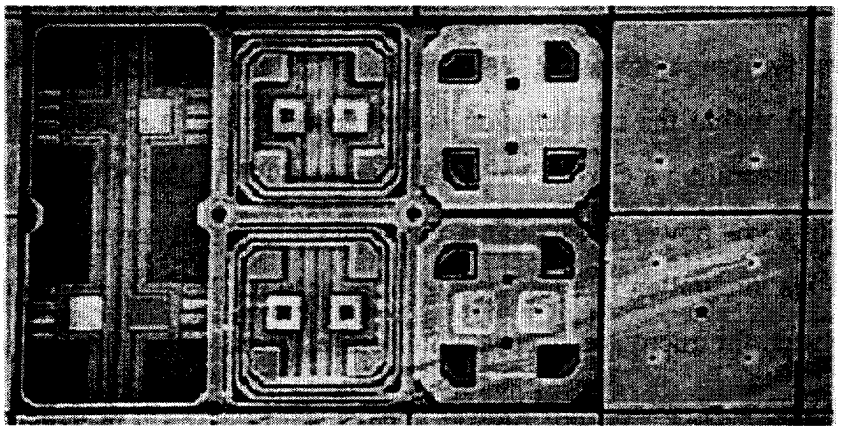

Figure 4.6 Details of the structure of the micro-mirrors are shown.

The adaptive optics telescope, using MOEMs micro-mirrors, facilitates extremely accurate tracking, and the ability - when coupled with a star-matching scheme based on algebraic coding theory - enables the capability to track at least 5 stars simultaneously. Moreover, the massively parallel architecture enables the star tracker to operate autonomously without burdening the spacecraft processor and may be used to supplement the onboard processor. Because the design utilizes technologies that inherently integrate well together and lend themselves to batch processing, estimations have that the Intelligent Star Tracker will have a recurring cost less than $100k. In addition to low cost, preliminary analysis indicates that the Intelligent Star Tracker will have a pointing accuracy exceeding 0.20 arc-sec, NEA better than 0.10 arc-sec, power consumption less than 2W and a weight of approximately 200 g.

e. DGPS

Formation flying will quickly revolutionize the way science, remote sensing and surveillance missions are performed in space, enabling a whole new range of applications for small satellites. Currently, there are numerous missions in the planning stages involving formation flying of a constellation of micro- or nanosatellites. However, to truly achieve the goals of these formation-flying missions, an accurate means of

relative ranging, determining time and position measurements, inter-satellite communications, and controlling the formation states is becoming critical. [Ref. 34]

The need of future formation flying missions to have technology with integrated capabilities for communicating, relative ranging, and exchanging precise timing among spacecraft within the constellation is fast approaching. AeroAstro Inc. is developed a system by integrating a Carrier Phase Differential GPS (CDGPS) navigation and attitude sensor with a low power, inexpensive, compact ranging and communications system. The result of this integration is a low-cost, robust, secure GPS micro navigation and communication system for micro and nanosatellite constellations called *Star Ranger.*

The ranging accuracy of *Star Ranger* is expected to be 1 cm or better, and the ultimate goal is set at 3 mm. Using CDGPS, it is expected that the relative attitude between spacecraft will be determinable to 0.5° or better. In addition, the overall relative position of each spacecraft with respect to each other will also be measurable to less than 1 cm, with a goal of 5 mm.

B. PROPULSION

There is an increasing need for on-board propulsion systems for micro- and nano-spacecraft. These include upper stage engines to boost spacecraft into final orbits as well as very small-scale boosters to launch new 1 kg class payloads for military, commercial and scientific applications.

Decreasing payload sizes will increase demand for smaller, more capable platforms, including the ability to maneuver and change orbit; hence the need for small propulsion systems. Such propulsive missions could include:

- Remote inspector to rendezvous and maneuver around a host spacecraft
- Constellations on the same launch vehicle requiring separation
- De-orbiting of space junk requiring rendezvous, docking and orbit changing

In addition to low cost, low mass and short delivery some more specific requirements for these propulsion systems include:

- Low power consumption
- Low, controllable thrust
- High propellant Isp
- High density Isp

The simplest spacecraft do not require thrust and hence have no propulsion equipment. But most spacecraft need some controlled thrust, so their design includes some form of metered propulsion – a propulsion system that can be turned on and off in small increments.

The propulsion system has three objectives. The first objective is to provide the remotes with attitude control, which involves rotational disturbance rejection and angular positioning. The second objective of the propulsion system is to enable formation flying. To maintain a formation with the mother center satellite, and other remotes, the propulsion system must have the ability to reject translational disturbances and reposition the remotes when the satellite drifts out of the formation. The third objective is to provide the ΔV necessary for the orbital maneuvers throughout the mission as determined by any mission plan. These maneuvers could include changing from one formation to another, changing orbital parameters, correct velocity errors, maneuver, counter disturbance forces (e.g., drag), control attitude during thrusting, and control and correct angular momentum.

The equipment in the propulsion subsystem includes a propellant supply (propellant, tankage, distribution system, pressurant, and propellant controls) and thruster or engines. Significant sizing parameters for the subsystem are the total impulse and number, orientation, and thrust levels of the thrusters.

1. Systems

a. Cold/Hot Gas

Cold-gas is a more traditional propulsion system. It provides thrust by expanding high-pressure gas through a nozzle. Some of the components required for the system are tank, tubing, filter, pressure regulator, valves, and thrusters. Currently the

GN&C's Propulsion Branch of the NASA's Goddard Space Flight Center (GSFC) is conducting a broad technology development program for propulsion devices that are ideally suited for nanosatellite missions. The goal of the program is to develop nanosatellite propulsion systems that can be flight qualified in a few years and flown in support of nanosatellite missions. The miniature cold gas thruster technology, the first product from the GSFC's propulsion component technology development program, will be flown on the upcoming ST-5 mission in 2003. The ST-5 mission is designed to validate various nanosatellite technologies in all major subsystem areas. It is a precursor mission to more ambitious nanosatellite missions such as the Magnetospheric Constellation mission. [Ref. 35]

b. MEMS

Small satellites flying in clusters require periodic "stationkeeping" to keep them in place. The required impulse is very small – the goal is not to keep the individual satellites in rigid formation, but only to keep them in well-defined orbitals with respect to one another. The necessary impulse, therefore, is only the amount needed to overcome the difference in drag between the most-affected and the least-affected satellites in the cluster. Estimates are that the differential drag can be overcome by providing ~1 mNsec (micro-Newton second) to ~1 mN sec (milli-Newton second) every 10 to 100 seconds throughout each satellite's mission.

Currently propulsion technology is developing rapidly towards miniaturized systems. Most notable is MEMS technology. The MEMS Mega-pixel Micro-thruster Array (see Fig. 4.7) thrusters have very low power and energy thresholds for ignition (~10 mWatts, ~100 μJoules), and no moving parts so are expected to be highly reliable. [Ref. 36] A single thruster array contains a quarter of a million separate thrusters.

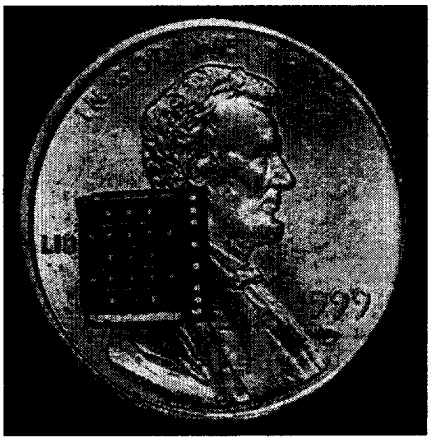

Figure 4.7 Aerospace MEMS chip compared to Penny

Marotta Scientific Controls is designing a very tiny Microelectromechanical System (MEMS) chip that provides fine attitude adjustments on the spacecraft; it uses 8.5 times less power and weighs 2 times less than proven attitude control systems. [Ref. 37] Marotta is also in the process of developing a unique microthruster (see Fig. 4.8) and electronics driver combination which is capable of low power operation (<1W peak), response time of $\leq$5 msec, minimum pulse rate of <1 Hz, and has a mass of 50g. The resulting low power component provides an order of magnitude reduction in solenoid coil heating when compared to an ordinary continuous duty solenoid valve. Aerospace, Primex, Honeywell and AFRL are working separately on MEMS based thrusters such as micro-hydrazine. These will be flown on numerous commercial and university based nanosatellite systems when the maturity of the technology will allow it. The small modular nozzles would allow many options as to microthruster size. Although development time will most likely require more than two years, the potential for nanosatellites is very high.

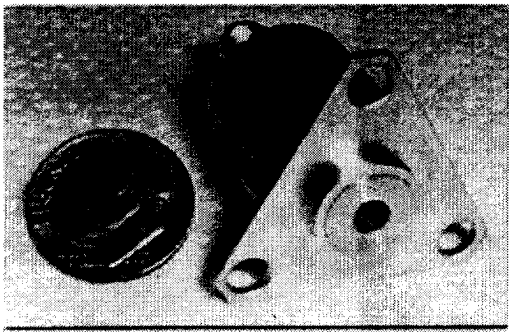

Figure 4.8 Marotta microthruster compared to Dime

c. Electrical

Primex Aerospace Company is working with the University of Washington to scale down the power requirements of their full-sized Pulsed Plasma Thrusters (see Fig. 4.9). The UW nanosatellite will fly a propulsion system, and will be either μPPT's, or a cold gas system.

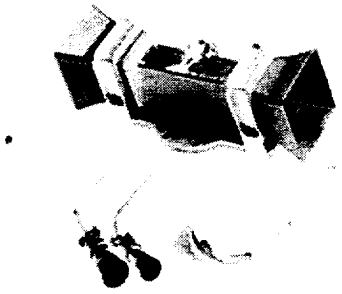

Figure 4.9 Full-sized Pulsed Plasma Thrusters from Primex Aerospace Company

A typical pulsed plasma thruster consists of two electrodes, a solid Teflon® propellant bar, an igniter (spark plug), a feed spring, a power supply, and a capacitor (shown in Fig. 4.10).

The power supply charges the capacitor, which is connected to the two electrodes. When a small plasma puff from the spark plug is released between the

electrodes, the puff creates a low-resistance arc path, discharging the energy stored in the capacitor. This arc ablates a small amount of the Teflon® propellant bar and turns part of it into plasma. The current flowing through the arc also creates a magnetic field, and the resulting JxB force accelerates the plasma away from the thruster, thus generating thrust.

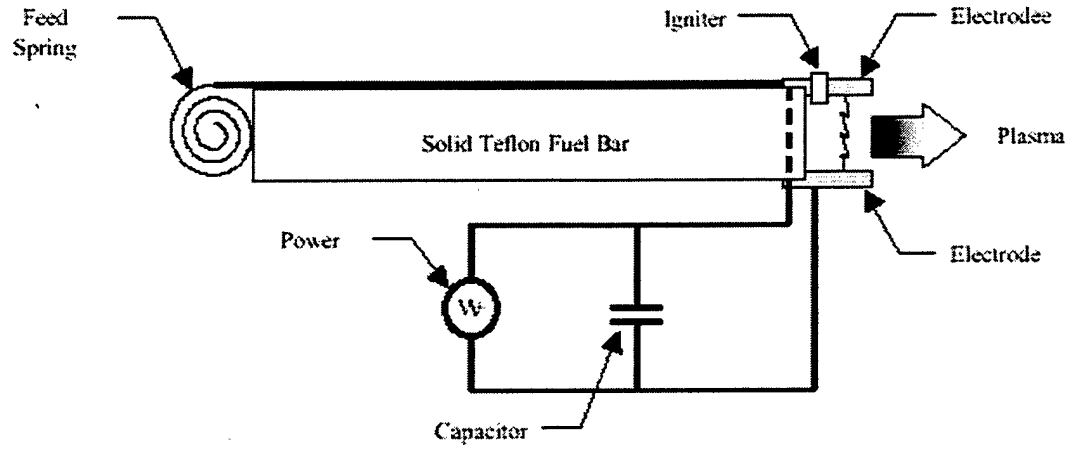

Figure 4.10 Basic diagram of a pulsed-plasma thruster

2. Performance

Three parameters determine the performance of a propulsion system. These three parameters are thrust (T), minimum impulse bit (I_{bit}), and specific impulse (I_{sp}). Given propulsion system hardware, the thrust can be measured experimentally. From these experimental data, the average thrust can be calculated. However, for a theoretical analysis, the thrust is calculated from Eq. (4.1):

$$T = \dot{m} \cdot C_{eff} \tag{4.1}$$

where $\dot{m}$ is the mass flow rate at the thruster exit and C_{eff} is the effective exhaust velocity.

The I_{bit} is the smallest amount of thrust that can be delivered by a thruster. This is given in the units of an impulse (force multiplied by time), such as 70 μNs. Although the I_{bit} may be calculated theoretically in some cases, it is usually calculated from the experimental data since the minimal thrusting capability depends highly on the

propulsion system hardware. The I_{bit} is calculated using Eqn. (4.2) from the thrust profile data of an experiment in which a propulsion system is activated for the shortest duration possible.

$$I_{bit} = \int_{t_i}^{t_f} T \cdot dt \tag{4.2}$$

In equation (4.2), t_i and t_f are the time at the start and the end of the thrusting, respectively. For the most spacecraft a low I_{bit} is desired for fine control of the attitude, and especially during dead-band limit cycling. The specific impulse is generally defined as shown in equation (4.3):

$$I_{sp} = \frac{T}{\dot{m} \cdot g_0} \tag{4.3}$$

where g_0 is the acceleration due to gravity at the surface of the Earth. The specific impulse is a measure of the amount of thrust a propulsion system can provide for a given propellant mass flow rate. The I_{sp} diminishes for most propulsion systems over their lifetime. The specific impulse is essentially a measure of the mass efficiency of a propulsion system, so a high I_{sp} is desired for the propulsion system.

3. Propulsion System Comparison (Cold gas / μPPT)

Two main propulsion systems were analyzed and compared. The results of the μPPT and cold-gas system performance analyses are summarized in Table 4.2 below.

Propulsion System Type	Total Mass (kg)	Isp (s)	Ibit (μNs)	T (mN)	Propellant Mass per ΔV (g-s/m)	ΔV Time Duration (s 2 /m)	Energy per ΔV (J-s/m)	Peak Power (W)
μPPT†	3.80	500	70	0.07	2	1.43×10^{5}	17.9×10^{6}	12.5
cold-gas	4.58	65	100	4.5	16	2.22×10^{3}	$1 \sim 5 \times 10^{4}$‡	10.1

† *The performance of the μPPT was analyzed assuming a 1 Hz firing frequency.*

‡ *The energy per ΔV requirement for a cold-gas thruster depends on the firing mode, pulsed or continuous.*

Table 4.2 Comparison of μPPT and cold-gas propulsion systems (single thruster performance).

Both μPPT and cold-gas thrusters provide enough thrust to compensate for maximum translational disturbances, due mostly to the remotes drag. The μPPT system has a lower mass due to its lower I_{bit} and higher I_{sp}, providing better pointing accuracy and more ΔV for a given propellant mass than the cold-gas system. The fine thrust control required for attitude control can be characterized by the long time duration per ΔV. Thus, an impulsive burn, or a short duration per ΔV burn, which is optimal for most orbital maneuvers, is of less importance. The peak power and energy consumption are high for μPPT systems.

Most importantly, μPPTs do not suffer from propellant leakage. Cold-gas systems have a history of failing due to propellant leakage. Compared to the cold-gas system's complexity and problems inherent to a high-pressure system and the limited miniaturization capability due to the flow characteristic of gases and liquids, the μPPT is more attractive. The μPPT has a simple feed system with minimal moving parts, leading to higher reliability. Also, μPPT system mass can be further reduced by decreasing the size of the electronics, the most massive component of the μPPT system. The μPPT characteristics are suited to small satellites and thus will become the stepping stone for future commercial nanosatellites that will utilize μPPTs.

EXAMPLE: SNAP-I (SSTL)

SNAP-1 is a low-cost nanosatellite built by Surrey Satellite Technology Ltd. SSTL), it is amongst other objectives a technology demonstrator for 3-axis stabilization nd orbit control for a future constellation of small satellites during formation flying. The atellite uses a single miniature Y-momentum wheel, 3-axis magnetic torquers and a ingle butane gas thruster to ensure a nominal nadir-pointing attitude with full pitch ontrol and in-track ΔV maneuverability. The magnetic torquers do momentum aintenance and nutation damping of the Y-wheel. The primary attitude sensor used, is a iniature 3-axis fluxgate magnetometer. Precise orbital knowledge was obtained using a mall single antenna GPS receiver supported by an on-board orbit estimator.

A low cost propulsion system was designed and built for the SNAP-1 spacecraft 1 7 months from concept to launch site. It utilizes butane stored as a liquid and operating 1 a cold gas mode. Miniature conventional technology was used for the valves. The ropellant was stored in a formed titanium tube, rather than a tank, giving a low cost olution. The spacecraft was loaded with 32.6 grams of butane prior to shipping it to aunch site. SNAP-1 was successfully launched on 28 June 2000.

The most obvious feature of the complete propulsion pipework assembly is that here was no propellant tank. The propellant was stored in 1.1 meter of coiled titanium ibe (see Fig. 4.11), providing 65 cm^3 of storage volume. [Ref. 38]

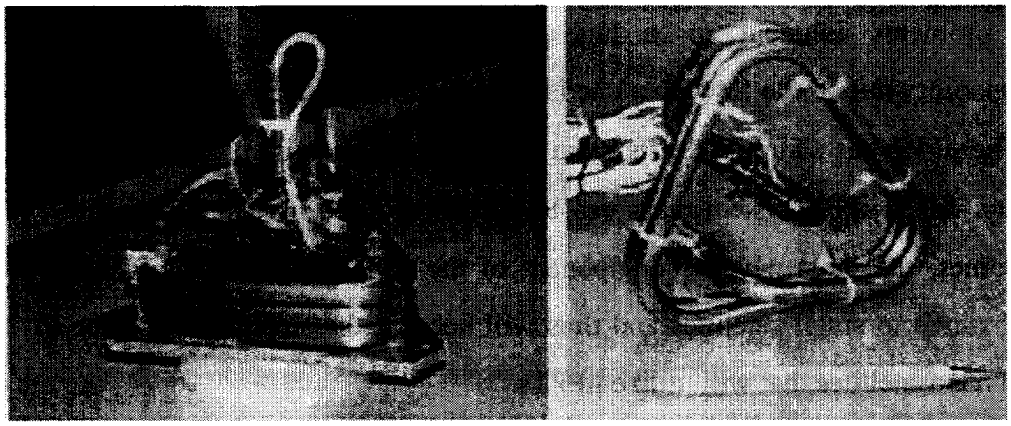

Figure 4.11 Snap-1 Propellant tube

V. CONCLUSION

A. THE NANOSATELLITE PUSH

In recent years, an increased effort to design, build, and operate small satellites has taken place in universities and laboratories all over the world. These microsatellites and nanosatellites provide numerous flight opportunities for science experiments at a fraction of the cost of larger traditional missions. This paper has presented an enormous thrust toward innovative ways, not only of satellite design, but a shift in thinking about satellite's roles and abilities in the coming years. Nanosatellites are far from being the 'some distant future', and indeed are not even the end of the line for this new movement in space commercialization. Picosatellites and femtosatellites are currently being designed and built, with space engineering paving the way for many powerful opportunities to show how useful and cunning these systems can be to both the commercial fields and to the military.

B. FORMATION DESIGNS

Imagine satellites numbering in the tens, hundreds or even thousands being launched off surface combatant ships, submarines, mobile Army vehicles or even Air Force cargo planes. The possibility of throwing a large quantity of 'sensors' quickly and efficiently into an engaged theater wherever/whenever removes the dependence on costly, vulnerable national-asset satellites.

The preceding chapters looked at the possibility of creating clusters that through their natural motion retain a constant shape when viewed from the planet's surface. It is shown that the shape of the apparent circular orbit can be described in terms of eccentricity of the orbit, and that terms through second order in e are sufficient to describe the motion to a high order of accuracy. Many formation designs have been presented to show that utilizing natural orbits allows formation dynamics to help reduce fuel requirements for formation-, and station-keeping needs. These natural orbits, coupled with robust control laws and precise position knowledge and inter-satellite

communication abilities, are key to the growing need and requirement for future NASA, DoD and commercial space missions.

C. PERTURBATION UPKEEP

This paper has presented the effects of the earth's oblateness on satellite formation flying designs like the circular and projected circular clusters. There are two components of motion that must be accounted for: 1) differential changes in the right ascension of the ascending node, and 2) secular changes in the argument of perigee and mean anomaly. The cost to maintain relative node spacing is dependent on the size of the formation. For a circular cluster of 25 km radius, the cost is approximately 7.2m/sec per year of velocity impulse. The cost to maintain the argument of perigee, not being a function of the cluster size, is roughly 2.1m/sec per year for the circular cluster. If the maneuvers cannot be coupled, a cluster like the one presented here could require close to 10m/sec per year of velocity impulse. Based on the orbit propagations and an assumed 10% error bounded on the formation, maneuvers would be required every 40 hours or so. Other perturbing effects may also require maneuvers but at far less frequency and cost than the oblateness induced maneuvers. It should also be pointed out that maneuvers may be required in all directions and each satellite in the formation must be able to thrust in the along-track, cross-track, and radial directions. The amount of formation keeping maneuvers will also vary from satellite to satellite within the formation.

Station keeping cost for the classes of orbits discussed here is relatively small. Only atmospheric drag decay of the semimajor axis is a major concern. Velocity impulse to correct for this effect is on the order of .097m/sec per year using high drag conditions.

Another major issue that impacts the frequency and cost of formation keeping maneuvers is that of attitude control. The formation keeping maneuvers discussed above require thrusting in the along-track, cross-track and radial directions. The satellite dynamics are very sensitive to acceleration in the along-track directions. The largest maneuvers are required in the cross-track and radial directions. If the satellite pointing has substantial errors when cross-track or radial maneuvers are performed, some unwanted acceleration might be applied in the along-track direction with significant

consequences. This will undoubtedly drive the frequency and cost of formation-keeping higher than what has been calculated here.

Orbit determination knowledge is another factor that will influence formation control. The STK's simulated propagations show that centimeter level differences in semimajor axis cause significant along-track error growth over time. The ability to determine the orbits to this level of precision is vital for precise and efficient formation control.

THIS PAGE INTENTIONALLY LEFT BLANK

APPENDIX 2.1

	Launched from	International Designator	Mass (g)	Initial orbit @ 51.6 deg	Decayed
Oderacs A	STS60 9Feb94	1994-006B	4200	225x463 km @ 51.6 deg	10 Feb 94
Oderacs B	STS60 9Feb94	1994-006C	4200	239x451 km @ 51.6 deg	10 Apr 94
Oderacs C	STS60 9Feb94	1994-006D	500		3 Mar 95
Oderacs D	STS60 9Feb94	1994-006E	500		6 Feb95
Oderacs E	STS60 9Feb94	1994-006F	5	266x272 km @ 51.6 deg	3 Mar 95
Oderacs F	STS60 9Feb94	1994-006G	5	266x271 km @ 51.6 deg	24 Feb 95
Oderacs 2A	STS63 4Feb95	1995-004C	5000	267x277 km @ 51.6 deg	13 Mar 1995
Oderacs 2B	STS63 4Feb95	1995-004D	4200	323x349 km @ 51.6 deg	29 Sep 1995
Oderacs 2C	STS63 4Feb95	1995-004E	500		7 Feb 1995
Oderacs 2D	STS63 4Feb95	1995-004F	1.5	314x320 km @ 51.6 deg	2 Mar 1995
Oderacs 2E	STS63 4Feb95	1995-004G	1.5	320x334 km @ 51.6 deg	27 Feb 1995
Oderacs 2F	STS63 4Feb95	Not catalogued by NORAD	0.5		20 Feb 1995

ODERACS Data Table

THIS PAGE INTENTIONALLY LEFT BLANK

APPENDIX 2.2

Educational institutions involved in small satellites

Increasingly, it is becoming possible for educational institutions to be involved in small satellites. This is largely due to affordable yet sophisticated technology. This then allows satellites to be designed and built within the course duration, or via a series of student projects.

The following list of educational establishements are those known to be involved in small spacecraft projects. This can be either in experiments, parts of satellites, or entire satellites. Where known, specific spacecraft project names apear in brackets, inclucing a year when launched (or expected to be launched). For more details on the projects, please refer to the satellite and future mission lists.

All the links on this page will lead you to the individual institutions

Europe

- Universidad Complutense, Madrid, Spain
- Universidad Politecnica de Madrid, Spain (UPMSAT '95)
- Surrey Space Centre University of Surrey, Surrey, United Kingdom (UoSAT series '80 onwards)
- Technical University of Helsinki in Finland (HUTSAT)
- University of Leicester, England (CATSAT)
- Technical University of Berlin, Germany (TUBSAT series '90 onwards)
- University of Bremen, Germany (BREMSAT '94, Abrixas '97)
- Royal Institute of Technology in Stockholm, Sweden. (KTHSat)
- Instituto Superior Técnico , Lisbon Portugal. (PoSAT-1)
- Unitersitaet Kaiserslautern, Germany (Phase 3D)
- Dept. of Space Physics of Umeå University (RYP) (Munin)

North America

In the U.S., NASA encourages participation in small missions via the University Explorer (UNEX) Programme.

- University of Illinois at Urbana-Champain.
- Stanford University, , U.S. (SAPHIRE and OPAL)
- Arizona State University, Tempe, Arizona, U.S. (ASUSAT)
- University of Arizona, Tuscon, U.S., Students Satellite Program (UASAT)
- Iowa State Univerity, Ames, Iowa, U.S. (ISAT)
- Universidad Nacional Autónoma de México, Mexico City, Mexico (UNAMSAT)

- Naval Postgraduate School, Monterey, California, U.S. (PANSAT)
- San Jose State University, San Jose, California, U.S. (SPARTNIK)
- Sierra Community College, Rocklin, California, U.S. (MINERVA)
- University of Alabama, Huntsville, Alabama, U.S. (SEDSAT)
- Utah State University, Logan, Utah, U.S. (NUSAT '85, Webersat etc CAST)
- Johns Hopkins University Applied Physics Laboratory, U.S.
- Penn State University, U.S. (SAC-B CUBIC instrument)
- University of Colorado, U.S.
- Massachusetts Institute of Technology Centre for Space Research, U.S. (HETE)
- Weber State Univerity, Ogden, Utah, U.S. (NUSAT '85, WEBERSAT '90 and more)
- University of New Hampshire, U.S. (CATSAT)
- Boston University, U.S. (TERRIERS)
- Anahuac University, Mexico (ANISAT Nano-satellite project)
- Carleton University, Canada. (SILA microsatellite)
- University of Toronto (MOST microsatellite)

Africa

- University of Stellenbosch, South Africa (SUNSAT)

Asia

- Korean Advanced Institute of Science /Technology (KAIST), S.Korea (KITSAT series)
- Mahanakorn University, Thailand (TMSAT)
- National Central University, Taiwan (TUU-Sat)
- ATSB, Malaysia, (TiungSAT)
- Tsinghua University, China (Tsinghua-1)

South America

- Universidad de La Frontera, Temuco, Chile, Involved with the design and construction of CESAR-1

APPENDIX 3.1

STK Screen Shots

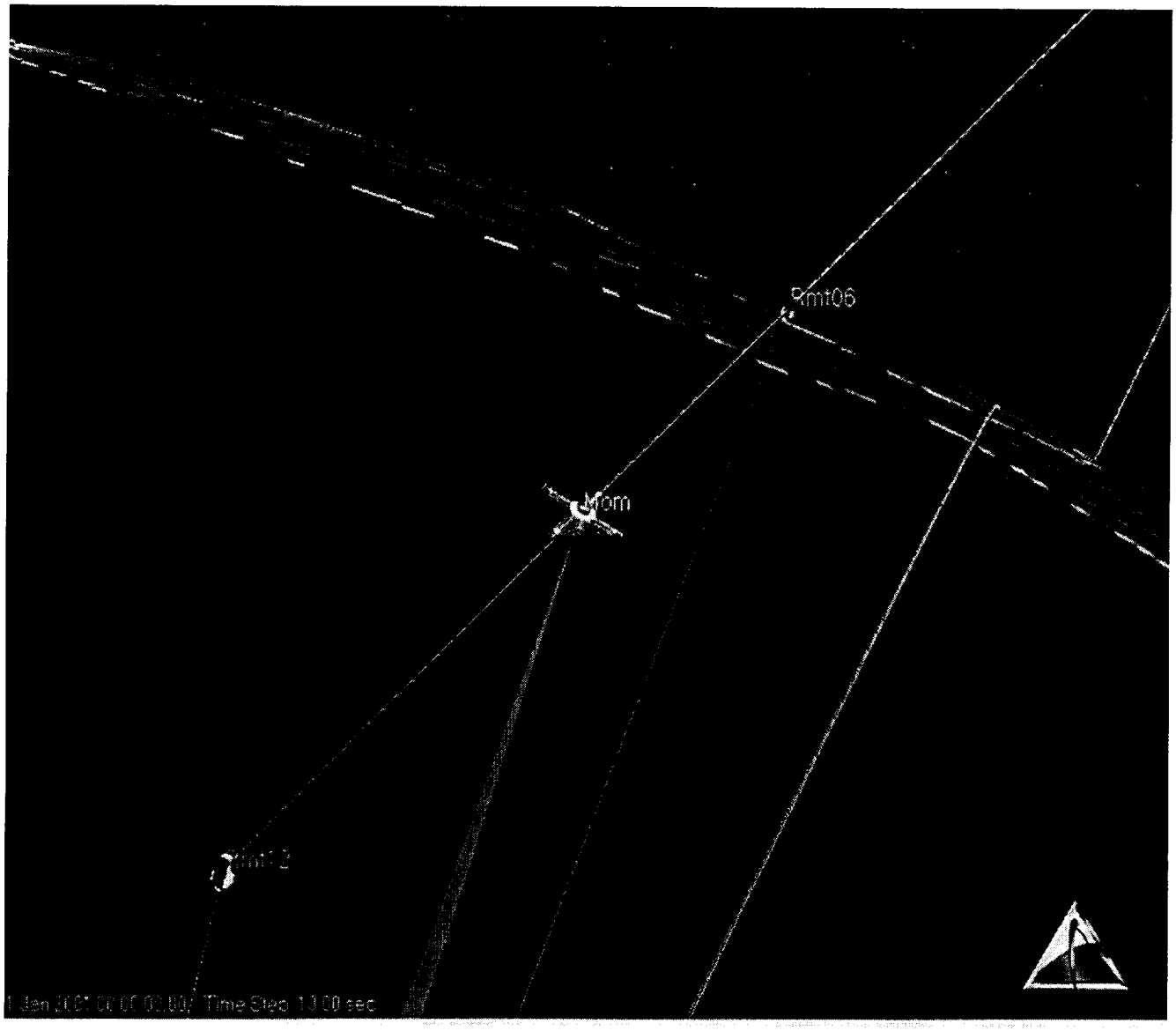

In-Track Formation(2 remotes)

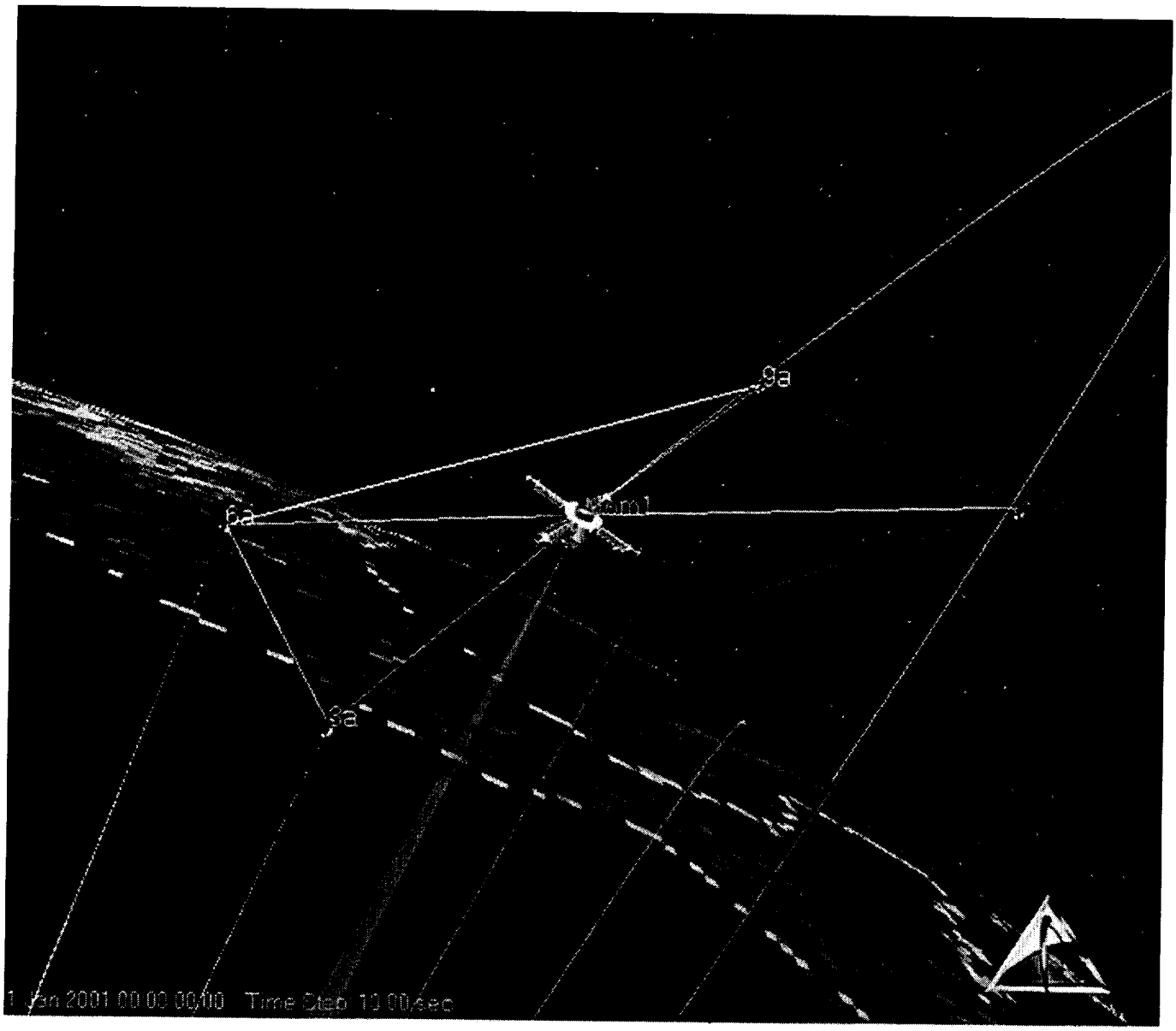

Circular Formation (4 remotes)

APPENDIX 3.2

Matlab Code for STK data input in inertial position/velocity parameters

```
%Cluster Formation
clear
clc
%Need Mother parameters
      %ac - semimajor axis
      %ec - eccentricity
      %ic - inclination
      %RAANc - right ascension of ascending node
      %argc - argument of perigee
      %Mc - mean anomaly at epoch
      %Ec - eccentric anomaly
      %Tc - true anomaly
      %rc - radius
      %vc - orbital speed
ac = 7489.137000; %km
ecdeg = 0.00;           %deg
ec = ecdeg*pi/180;      %rad
icdeg = 63.4;           %deg
ic = icdeg*(pi/180);    %rad
RAANcdeg = 0;           %deg
RAANc = RAANcdeg*pi/180;%rad
argcdeg = 0;            %deg
argc = argcdeg*pi/180;  %rad
pc = ac*(1-ec^2);
mu = 398600.5;          %km^3 s^-2


%Cluster geometry parameters
      %rho - scale factor; determines overall cluster size/ assigned
      same for all subsats
      %nu - dimensionless pattern generator; determines geometrical
      arrangement
      %delta - angle; specifies shape of suborbit & orientation of
      suborbit plane wrt centersat orbit
```

```
      %rs = subsat radial speed
      %vs = subsat orbital speed
      %as = subsat semimajor axis

rho = 100;                    %km
deltadeg = 63.4;              %deg
delta = deltadeg*pi/180;      %rad
as = ac;                      %km

%First choose eccentric anomaly, Ec, of centersat
      numsats=8
      for m=0:numsats-1
          Ec=(2*pi/numsats*m);          %Eccentric Anomaly - Equal
spacing circular

          %Pattern Generator for Desired Pattern
          nu=.5;              %Circular Spacing, one loop

%Calculte Center-Sat parameters
Tc=2*atan(sqrt((1+ec)/(1-ec))*tan(Ec/2));
Mc=Ec-ec*sin(Ec);
rc=pc./(1.+ec.*cos(Tc));
vc=sqrt(mu*(2/rc-1/ac));

%Calculte Sub-Sat parameters (use 12 o'clock insertion position)
as=ac;      %Assumed for all subsats
rs=sqrt((nu*rho*sin(delta))^2+(rc+nu*rho*cos(delta))^2);
vs=sqrt(mu*(2/rs-1/as));

%Calculate Vectors
Rc=rc*[cos(Tc) sin(Tc) 0]';
Vc=sqrt(mu/pc)*[-sin(Tc) ec+cos(Tc) 0]';

Rs=[(rc+nu*rho*cos(delta))*cos(Tc)          (rc+nu*rho*cos(delta))*sin(Tc)
nu*rho*sin(delta)]';
Vs=vs/vc.*Vc;
```

```
%Transform subsat radius/velocity vectors from centersat coord to
Earth-centered inertial coord
Rxx = 3x3 rotation matrix from RSW to IJK frame
Rraanc = [cos(-RAANc) sin(-RAANc) 0; -sin(-RAANc) cos(-RAANc) 0; 0 0
1];
Ric = [1 0 0; 0 (cos(-ic)) (sin(-ic)); 0 (-sin(-ic)) (cos(-ic))];
Rargc = [cos(-argc) sin(-argc) 0; -sin(-argc) cos(-argc) 0; 0 0 1];


R = Rraanc*Ric*Rargc;


Rijk=R*Rs
Vijk=R*Vs


Rsub(m+1,1:numsats-1)=Rijk';
Vsub(m+1,1:numsats-1)=Vijk';


%Calculate Orbital Elements
%As should equal Ac for all subsats (Assumed)


end


display('SubSat1');
```

THIS PAGE INTENTIONALLY LEFT BLANK

APPENDIX 3.3

Example orbital Parameters from Matlab to STK coordinate transformation

	Orbital Parameters	$\delta = 0$	$a_c = 6978.137$ km	alt = 600 km	Ring radius ~25 km	
MOM	**63.4**	**0**	**0**	**0**	**0**	
Position	*Inclination*	*Eccentricity*	*Arg*	*RAAN*	*Mean Anomaly*	
0	63.4	0.003	180	-0.006913 deg	180	Top
1.5	63.403457 deg	0.003	225.012421 deg	0	134.987579 deg	
3	63.406913 deg	0.003	270.024842 deg	0.000001 deg	89.975158 deg	
4.5	63.403457 deg	0.003	315.012421 deg	0	44.987579 deg	
6	63.4	0.003	0.006913 deg	0	0	Bottom
7.5	63.396543 deg	0.003	44.987579 deg	0	315.012421 deg	
9	63.393087 deg	0.003	89.975158 deg	-0.000001 deg	270.024842 deg	
10.5	63.396543 deg	0.003	134.987579 deg	0	225.012421 deg	
12	63.4	0.003	180	-0.006913 deg	180	

For second outer ring: e=.006 (all other parameters stay the same)

	Orbital Parameters	$\delta = 63.4$	$a_c = 6978.137$ km	alt = 600 km	Ring radius ~25 km	
MOM	**63.4**	**0**	**0**	**0**	**0**	
Position	*Inclination*	*Eccentricity*	*Arg*	*RAAN*	*Mean Anomaly*	
0	63.400654	0.00328833	0.211983 deg	359.630879 deg	359.953493 deg	Top
1.5						
3	63.06986	0.00325885	270 deg	0 deg	0 deg	
4.5						
6	63.400654	0.00328833	179.788017 deg	0.369121 deg	0.046908 deg	Bottom
7.5						
9	63.730337	0.00326474	90 deg	0 deg	0 deg	
10.5						
12	63.400654	0.00328833	0.211983 deg	359.630879 deg	359.953493 deg	

For second outer ring: e=.006 (all other parameters stay the same)

	Orbital Parameters	δ = 63.4	a_c = 7489.137 km	alt = 1111 km	Ring radius ~23 km	
MOM	**63.4**	**0**	**0**	**0**	**0**	
Position	*Inclination (°)*	*Eccentricity*	*Arg (°)*	*Ω (°)*	*M (°)*	
0	63.400508	0.00300701	180.170765	359.61862	180	Top
1.5						
3	63.058986	0.00300701	90	0 deg	180	
4.5						
6	63.400508	0.00300701	359.829235	0.38138	180	Bottom
7.5						
9	63.741014	0.00300701	270	0 deg	180	
10.5						
12	63.400508	0.00300701	180.170765	359.61862	180	

For second outer ring: e=.006 (all other parameters stay the same)

APPENDIX 3.4

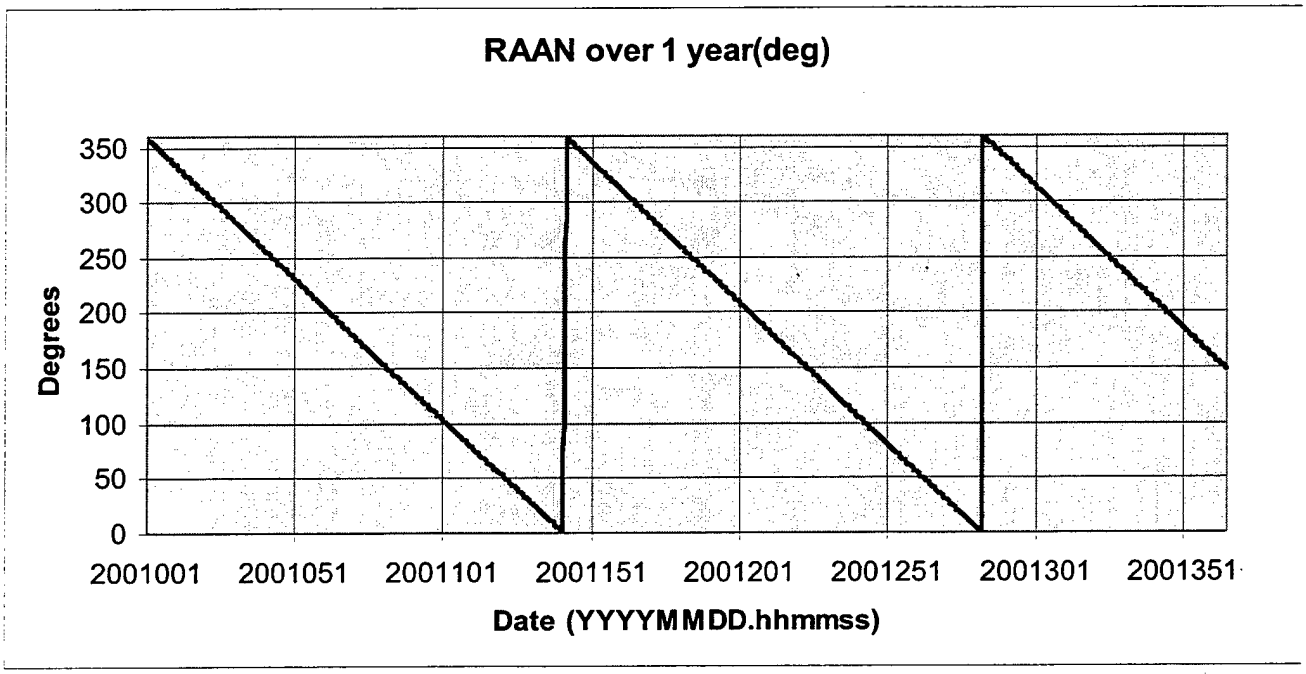
RAAN over 1 year(deg)
Degrees
350
300
250
200
150
100
50
0
2001001
2001051
2001101
2001151
2001201
2001251
2001301
2001351
Date (YYYYMMDD.hhmmss)

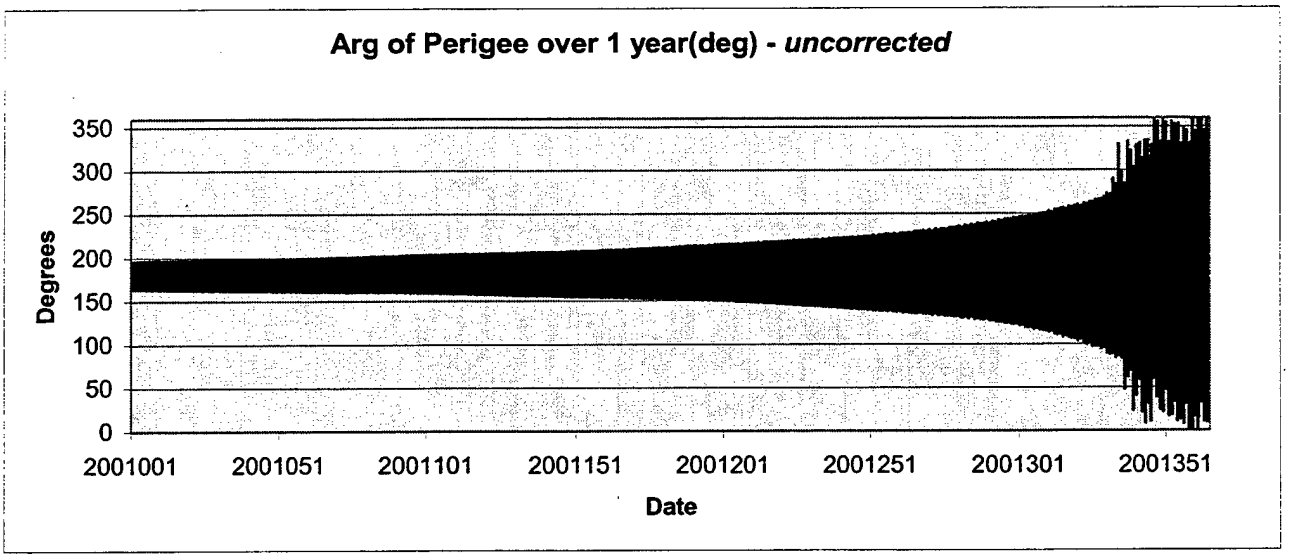
Arg of Perigee over 1 year(deg) - *uncorrected*
Degrees
350
300
250
200
150
100
50
0
2001001
2001051
2001101
2001151
2001201
2001251
2001301
2001351
Date

THIS PAGE INTENTIONALLY LEFT BLANK

APPENDIX 4.1

Sensor	Performance	Mass (kg)	Power (W)	Unit Price	Units	Notes
Micro-Gyroscope	0.004°/s short-term bias and resolution	0.060	0.030	$450	1	Use between magnetometer measurements. Must be zeroed out regularly using the magnetometer.
Magnetometer	~ ±3° attitude	0.018	0.030	$2200	1	Nominal use is for yaw attitude only. Can be used for three-axis attitude if necessary.
Reaction Wheel	8300-8400 rpm 0.015 Nms	0.450	2.0	Built by HIT	3	
Horizon sensor	±1° attitude	0.113	0.030	$40,000	2	Pitch and roll attitude
Star Tracker	pointing accuracy: 0.20arcsec NEA: better than 0.10arcsec	0.200	< 2.0	$100,000	1	Tracker's processor may be used to supplement onboard processor
TOTALS		0.954	4.120	$182,700	8	

Comparison of attitude sensors

THIS PAGE INTENTIONALLY LEFT BLANK

LIST OF REFERENCES

1. Daniel S. Goldin, Administrator of National Aeronautics and Space Administration before the Subcommittee on VA, HUD and Independent Agencies Committee on Appropriations House of Representatives, March 15, 2000.
2. Online World Wide Web (WWW), http://www.amsat.org/, March 17, 2001.
3. Online WWW, http://www.nas.nasa.gov/Pubs/NASnews/95/11/nanotech.html, April 09, 2001.
4. Explorer satellite on Astronautix website, online WWW, http://www.friends-partners.org/mwade/craft/exporera.htm, March 15, 2001.
5. Vanguard satellite homepage, online WWW, http://home5.swipnet.se/~w-52936/index20.htm, March 15, 2001.
6. Online WWW, http://www.itu.int/home/index.html, March 15, 2001.
7. Online WWW, http://screem.engr.scu.edu/artemis, March 15, 2001.
8. Online WWW, http://www.estec.esa.nl/outreach/sseti/homepage.htm, March 15, 2001.
9. Online WWW, http://www.nanosat.usu.edu/overview/3corner.html, March 15, 2001.
10. Online WWW, http://www.nanosat.usu.edu/overview/ion-f.html, March 15, 2001.
11. Online WWW, http://www.nanosat.usu.edu/overview/emerald.html , March 15, 2001.
12. Online WWW, http://www.aa.washington.edu/faculty/campbell/dawgstar/dawgstar.htm, March 15, 2001.
13. Online WWW, http://www.osss.com, March 15, 2001.
14. Sabol, Chris, Burns, Richard, McLaughlin, Craig A., *Satellite Formation Flying Design and Evolution*, AAS 99-121.
15. Kapila, Vikram, Sparks, Andrew G., Buffington, James M., Yan, Qiguo, *Spacecraft Formation Flying: Dynamics and Control*, Journal of Guidance, Control, and Dynamics, Vol. 23, No 3, pg 561, 2000.
16. Folta, D.C., Newman, L.K., Gardner, T., *Foundations of Formation Flying for Missions to Planet Earth and New Millennium*, AIAA/AAS Astrodynamics Conference, San Diego, Jul 29-31, 1996. AIAA 97-3645-CP.

17. TechSat 21 Space Missions Using Satellite Clusters, Air Force Research Lab Space Vehicles Directorate Factsheet from WWW, http://www.vs.afrl.af.mil/factsheets/techsat21.html.

18. McInnes, C.R., *Autonomous Ring Formation for a Planar Constellation of Satellites*, Journal of Guidance, Control, and Dynamics, Vol18, No. 5, 1995, pp. 1215-1217.

19. Chao, C. C., Pollard, J. E., and Janson, S.W., *Dynamics and Control of Cluster Orbits for Distributed Space Missions*, Proceedings of the AAS Space Flight Mechanics Meeting, AAS99-126, Publication, Washington, DC, 1999.

20. Mallory, Jilla, and Miller, Optimization of Geosynchronous Satellite Constellations for Interferometric Earth Imaging, 1998.

21. Vallado, David A., *Fundamentals of Astrodynamics and Applications*, published as part of the Space Technology Series by the McGraw-Hill Companies, Inc., College Custom Series, 1997.

22. Frauenholz, R.B., *An Analysis of the TOPEX/POSEIDON Operational Orbit: Observed Variations and Why*," AAS Paper 95-366, Aug 1995.

23. Battin, Richard H., *An Introduction to the Mathematics and Methods of Astrodynamics*, AIAA Education Series, published by the American Institute of Aeronautics and Astronautics, Inc., New York, NY, 1987.

24. Stickler, A. C., and Alfriend, K. T., *Elementary Magnetic Attitude Control System*, Journal of Spacecraft and Rockets, Vol. 13, No. 5, 1976, pp. 282-287.

25. Alfriend, K. T., *Magnetic Attitude Control System for Dual-Spin Satellites*, AIAA Journal, Vol. 13, No. 6, 1975, pp. 8172-822.

26. Siahpush, A., and Gleave, J., *A Brief Survey of Attitude Control Systems Utilizing Momentum Wheel Concepts for Small Satellites*, Proceedings of the 1st Utah State University Conference on Small Satellites, Center for Space Engineering, Logan, UT, 1988.

27. Grassi and Pastena, *Minimum Power Optimum Control of Microsatellite Attitude Dynamics*, Journal of Guidance, Control and Dynamics Vol 23, No 5, pg 798 – 804, 2000.

28. Navid Yazdi, Farrokh Ayazi, Khalil Najafi, *Micromachined Inertial Sensors*, Proceedings of the IEEE, Vol. 86, August 1998, pp. 1640-1659.

29. Systron Donner, BEI Gyrochip TM Micromachined Angular Rate Sensor, online WWW, http://www.systron.com/prodinfo/QRS11.html.

30. Litton G2000 gyroscope, online WWW, http://www.littongcs.com/products/2guidance/traditional/g2000/tech.html.

31. Applied Physics Systems, *Model 533 Miniature 3 Axis Fluxgate Magnetometer*, online WWW, http://www.appliedphysics.com/left_navigation_pages/model_type/active_pane/model533D.html.

32. EDO Barnes, Model 13-500 – Wide-Angle, Miniature, Solid-State Horizon Sensor, online WWW, http://www.nycedo.com/edocorp/defense/optics/products/13-500.html.

33. Natalie Clark, Paul Furth, and Steven Horan, *Intelligent Star Tracker*, Proceedings of 14th Annual Small Satellite AIAA/Utah State University, SSC00-III-1, Aug 21-24, 2000.

34. Ray Zenick, and Kimberly Kohlhepp, *GPS Micro Navigation and Communication System for Clusters of Micro and Nanosatellites*, Proceedings of 14th Annual Small Satellite AIAA/Utah State University, SSC00-VI-8, Aug 21-24, 2000.

35. M.S. Rhee, C.M. Zakrzwski, M.A. Thomas, *Highlights of Nanosatellite Propulsion Development Program at NASA-Goddard Space Flight Center*, Proceedings of 14th Annual Small Satellite AIAA/Utah State University, SSC00-X-5, Aug 21-24, 2000.

36. Daniel W. Youngner, Son Thai Lu, Edgar Choueiri, Jamie B. Neidert, Robert E. Black III, Kenneth J. Graham, Dave Fahey, Rodney Lucus, Xiaoyang Zhu, *MEMS Mega-pixel Micro-thruster Arrays for Small Satellite Stationkeeping*, Proceedings of 14th Annual Small Satellite AIAA/Utah State University, SSC00-X-2, Aug 21-24, 2000.

37. Marotta Scientific Controls, online WWW, http://www.marotta.com/microthrust.asp.

38. D Gibbon, Dr. J Ward, N.Kay, *The Design, Development and Testing of a Propulsion System for the SNAP-1Nanosatellite*, Proceedings of 14th Annual Small Satellite AIAA/Utah State University, SSC00-I-3, Aug 21-24, 2000.

Challa, M., Natanson, G., Deutschmann, J., and Galal, K., *A PC-based Magnetometer-Only Attitude and Rate Determination System for Gyroless Spacecraft*, presented at the GSFC FDD Flight Mechanics Estimation Theory Symposium, Paper No. 07, NASA Goddard Space Flight Center, Greenbelt, Maryland, May 16-18, 1995, pp. 83-96.

DeCou, A. B., *Orbital Station-Keeping for Multiple Spacecraft Interferometry*, Journal of Astronautical Sciences, Vol. 39, July-Sept, 1991, pp. 283-297.

Eterno, John S., Zermuehlen, Robert O., Zimbelman, Harold F., *Attitude Determination and Control*, Space Mission Analysis and Design, edited by Wiley J. Larson and James R. Wetrz, 2nd edition. Space Technology Series, Microcosm, Inc, & Kluwer Academic Publishers, 1992, pp. 340-366

Folker, W.M., et al, *LISA Orbit Selection and Stability*, Classical and Quantum Gravity, Volume 14, pp 1405-1410, 1997.

Hill, G.W., *Researches in the Lunar Theory*, American Journal of Mathematics, Volume 1, pp 5-26, 1878.

Kang, Sparks and Banda, *Coordinated Control of Multisatellite Systems*, Journal of Guidance, Control and Dynamics, pg 360, 2000.

Mallory, Jilla, and Miller, Optimization of Geosynchronous Satellite Constellations for Interferometric Earth Imaging, 1998.

Ovchinnikov, M., Yu., *Simple Methods of Attitude Control for Small Satellites*, International Academy of Astonautics, Paper 95-IAA.11.2.08, Oct 1995.

Roux, Alain, *Cluster Regroups for Relaunch*, Aerospace America, pp. 48-51, August 1998.

Sabol, Burns and McLaughlin, *Satellite Formation Flying Design and Evolution*, Proceedings of the AAS Space Flight Mechanics Meeting, AAS99-121, Washington, DC, 1999.

Siahpush, A., and Sexton, A., *A Study for Semi-passive Gravity Gradient Stabilization of Small Satellites*, Proceedings of the 1st Utah State University Conference on Small Satellites, Center for Space Engineering, Logan, UT, 1987.

Wang, P., Hadaegh, F., and Lau, K., *Synchronized Formation Rotation and Attitude Control of Multiple Free-Flying Spacecraft*, Journal of Guidance, Control, and Dynamics, Vol. 22, No. 1, 1999, pp. 28-35.

INITIAL DISTRIBUTION LIST

1. Defense Technical Information Center 2
   8725 John J. Kingman Rd., STE 0944
   Ft. Belvoir, VA 22060-6218

2. Dudley Knox Library 2
   Naval Postgraduate School
   411 Dyer Road
   Monterey, CA 93943-5101

3. Department Chairman, Code AA 1
   Department of Aeronautics and Astronautics
   Naval Postgraduate School
   699 Dyer Road, Rm. 137
   Monterey, CA 93943-5106

4. Dr. Brij N. Agrawal, Code AA/AB 1
   Department of Aeronautics and Astronautics
   Naval Postgraduate School
   699 Dyer Road, Rm. 137
   Monterey, CA 93943-5106

5. Dr. Alfred N. Sorenson, Aerospace Corp. 1
   P.O. Box 92957-M1/065
   Los Angeles, CA 90009-2957

6. SRDC Research Library, Code AA 1
   Department of Aeronautics and Astronautics
   Naval Postgraduate School
   699 Dyer Road, Rm. 137
   Monterey, CA 93943-5106

7. Stephen Tomlin 2
   3910 Red Leaf Ct.
   Point of Rocks, MD 21777

8. Sterling-Ann Tomlin 1
   4085 Mt View Rd
   Hays, NC 28635

9. Douglas Tomlin 1
   Singing Waters Lane
   Purlear, NC 28665